MASARYKOVA UNIVERZITA

PŘÍRODOVĚDECKÁ FAKULTA

Metody hledání period ve světelných křivkách tumblerů

Diplomová práce

SAMUEL BURANSKÝ

Brno, jaro 2025

MASARYKOVA UNIVERZITA

PŘÍRODOVĚDECKÁ FAKULTA

Metody hledání period ve světelných křivkách tumblerů

Diplomová práce

SAMUEL BURANSKÝ

Vedoucí práce: Mgr. Tomáš Henych, Ph.D.

Ústav teoretické fyziky a astrofyziky

Brno, jaro 2025

MUNI
PŘÍRODOVĚDECKÁ
FAKULTA

Bibliografický záznam

Autor:	Samuel Buranský Přírodovědecká fakulta Masarykova univerzita Ústav teoretické fyziky a astrofyziky
Název práce:	Metody hledání period ve světelných křivkách tumblerů
Studijní program:	Fyzika
Obor:	Astrofyzika
Vedoucí práce:	Mgr. Tomáš Henych, Ph.D.
Akademický rok:	2024/2025
Počet stran:	xviii + 71
Klíčová slova:	asteroid, tumbler, světelná křivka, genetické algoritmy, periodogram, frekvence …

Bibliographic record

Author:	Samuel Buranský Faculty of Science Masaryk University Department of theoretical physics and astrophysics
Title of Thesis:	Methods for finding periods in light curves of tumblers
Degree Programme:	Physics
Field of Study:	Astrophysics
Supervisor:	Mgr. Tomáš Henych, Ph.D.
Academic Year:	2024/2025
Number of Pages:	xviii + 71
Keywords:	asteroid, tumbler, light curve, genetic algorithms, periodogram, frequency …

Abstrakt

V této práci jsem se zabýval různými metodami hledání frekvencí rotace a precese tumblerů v jejich světelných křivkách. Zkoumal jsem klasický Fourierův periodogram, CLEAN Fourierův periodogram, Lomb-Scarglův periodogram a fitování pomocí genetického algoritmu. Zaměřil jsem se také na obtíže při hledání rotačních a precesních frekvencí v periodogramech tumblerů, jako jsou aliasing, šum a projevy násobků nebo lineárních kombinací správných frekvencí. V této práci jsem zmiňované metody implementoval a otestoval na různých syntetických světelných křivkách asteroidů rotujících kolem hlavní osy, ale především na tumblerech. Používal jsem umělé světelné křivky s různými charakteristikami, jako jsou délka pozorování nebo vzorkovací frekvence. Výsledkem je, že hledání prvního odhadu frekvencí pomocí periodogramu je vhodné pro zmenšení velikosti parametrického prostoru pro vyhledávání pomocí genetického algoritmu. Pro jednoznačnost frekvencí je ale nutné tyto frekvence otestovat a prokázat fyzikálním modelováním rotace.

Abstract

In this thesis, I examined the various methods for searching for the frequencies (periods) of the rotation and precession of tumbling asteroids in their light curves. I examined the classical Fourier periodogram, the CLEAN Fourier periodogram, the Lomb-Scargle periodogram, and the genetic algorithm fitting. I also examined the difficulties in searching for the rotation and precession frequencies in the tumbler's periodogram, such as aliasing, noise, manifestation of multiples, or linear combinations of the proper frequencies. In this thesis, I implemented these methods and tested them on various synthetic light curves of the principal axis rotator, and then on light curves of several tumblers. I used an artificial light curve with various characteristics, such as length and sampling. The result is that searching for the first guess of the frequencies in the periodogram is good for decreasing the size of the parametric space for the genetic algorithm search. However, for the unambiguity of the frequencies, it is necessary to test and prove this frequency by the physical modeling of the rotation.

MUNI
SCI

MASARYKOVA UNIVERZITA
PŘÍRODOVĚDECKÁ FAKULTA
KOTLÁŘSKÁ 2, 611 37 BRNO
IČ: 00216224
DIČ: CZ00216224

ZADÁNÍ DIPLOMOVÉ PRÁCE

Akademický rok: 2023/2024

Ústav:	Ústav teoretické fyziky a astrofyziky
Student:	Bc. Samuel Buranský
Program:	Fyzika
Specializace:	Astrofyzika

Ředitel *ústavu* PřF MU Vám ve smyslu Studijního a zkušebního řádu MU určuje diplomovou práci s názvem:

Název práce:	Metody hledání period ve světelných křivkách tumblerů
Název práce anglicky:	Methods for finding periods in light curves of tumblers
Jazyk závěrečné práce:	angličtina

Oficiální zadání:
Among the small Solar System bodies, there are also free-precessing asteroids and cometary nuclei. Their light curves are more complex than those of ordinary asteroids and thus pose a challenge to derive parameters describing the asteroid's or comet's rotation and dynamical properties. In this thesis, the student will focus on the analysis of synthetic light curves of tumblers of varying quality simulating real photometric observations at different geometries. He/she will use the Lomb-Scargle periodogram corrected for observational aliasing, fit the light curve using genetic algorithms, and compare the found periods with the real ones. They will also compare the effectiveness of the approach with the brute force method.

Vedoucí práce:	Mgr. Tomáš Henych, Ph.D.
Datum zadání práce:	4. 12. 2023
V Brně dne:	11. 3. 2024

Zadání bylo schváleno prostřednictvím IS MU.

Bc. Samuel Buranský, 11. 12. 2023
Mgr. Tomáš Henych, Ph.D., 18. 12. 2023
Mgr. Dušan Hemzal, Ph.D., 21. 12. 2023

Poděkování

V prvom rade by som rád poďakoval vedúcemu práce Tomášovi Henychovi za neustálu pomoc, podporu a cenné rady počas tvorby tejto práce. Za jazykovú korektúri patrí veľká vďaka Paťke, ktorá bola ochotná si prečítať ďalšiu moju záverečnú prácu. Tomovi ďakujem za pomoc pri zefektívnení môjho programovania a za to, že mi ukázal čaro a užitočnosť verzovacieho systému Git prijateľným spôsobom.

Za neustálu podporu počas celého štúdia a najmä náročného záveru patrí obrovské ďakujem mojej priateľke Veronika. Za celoživotnú podporu a zázemie, bez ktorého by nebolo náročné štúdium možné, ďakujem svojej rodine aj všetkým kamarátom a známym.

Za to, kam som sa dostal, v neposlednom rade patrí vďaka učiteľom, ktorí ma sprevádzali cestou vzdelávaním, konkrétne Miroslav Mesaroš, ktorý vo mne na základnej škole spustil vášeň k vesmíru, Anna Uhríková a Mária Bašistová, ktoré ma podporovali v rozvoji v matematike a fyzike aj v ťažkých chvíľach počas štúdia na gymnáziu. Z učiteľov na univerzite by som rád spomenul menovite hlavne Filipa Hrocha za odovzdané praktické zručnosti z astronómie a astrofyziky.

Ďalej mi nedá nespomenúť mojich kolegov a kamarátov z mojej práce na brnenskej hvezdárni, mojich spolužiakov a kamarátov zo školy za veľmi príjemnú a priateľskú atmosféru počas celých piatich rokov štúdia a mojich spoluorganizátorov, kolegov a kamarátov z astronomickej olympiády.

Prohlášení

Prohlašuji, že jsem svoji diplomovou práci vypracoval samostatně pod vedením vedoucího práce s využitím informačních zdrojů, které jsou v práci citovány.

V Brně dne 6. 5. 2025 Samuel Buranský

Contents

Introduction

Small Solar System bodies, including asteroids, comets, meteoroids, and smaller bodies, are essential components of the Solar System. Due to high collision rates and low gravitational fields, these bodies are remnants from the early eras of the Solar System. Studying the asteroids teaches us a lot about the Solar System's history.

Most asteroid rotations are single-periodic (it implies their relaxed rotation for typical short-period asteroids[1]). These asteroids rotate around an axis with a maximal moment of inertia, corresponding to the shortest axis. Some asteroids exhibit an excited rotational state, such as precession or free precession. These precessing asteroids, like asteroids that rotate around their principal axes, encode all necessary information in their light curves. However, a larger parametric space is required to fully describe their rotation, necessitating eight dynamic parameters for a complete characterization. Two periods are present in the light curve of precessing asteroid (tumbler[2]), the rotational period P_ψ and the mean precession period around the angular momentum vector $\vec{L}$, P_ϕ defined by Δ_ϕ

$$P_\phi = 2\pi \frac{P_\psi}{\Delta_\phi}, \tag{1}$$

and precession angle ϕ changes by the amount Δ_ϕ during time interval P_ψ (Kaasalainen, 2001).

The physical motion of an asteroid can be described by its kinetic energy and angular velocity. The rotational motion is described by

$$\vec{L} = \hat{I}\vec{\omega}, \tag{2}$$

---

1. The thing is that all asteroids tend to have relaxed rotation. This damping scale is approximately given by the equation $\tau \sim \frac{\mu Q}{\rho K_3^2 r^2 \omega^3}$, where μ is the rigidity of the material, Q is the ratio of lost energy per cycle to the total rotational energy, ρ is the bulk density, K_2^3 numerically describes irregularity, r is the mean radius and ω is the angular rotational frequency. The typical damping scale is thousands or millions of years, but can be billions of years for slowly rotating ones (A. W. Harris, 1994).
2. The term "tumbling asteroids" for the non-principal axis rotation was firstly used in (A. W. Harris, 1994).

where $\vec{L}$ is the asteroid's angular momentum, $\vec{\omega}$ is the angular velocity, and $\hat{I}$ is the inertia tensor, which has six independent components in general. For the convenient choice of the coordinate system, we get zero non-diagonal elements of the matrix. Then diagonal components, $I_1 \leq I_2 \leq I_3$, are principal moments of inertia. In general, the rotational energy is given as

$$E = \frac{1}{2}\vec{\omega}^T \hat{I}\vec{\omega}\,, \tag{3}$$

and for the principal inertia coordinate system, we get

$$E = \frac{1}{2}\left(I_1\omega_1^2 + I_2\omega_2^2 + I_3\omega_3^2\right)\,, \tag{4}$$

where only I_1, I_2, I_3 are the non-zero diagonal components of the inertia tensor (Pravec et al., 2005). Depending on the values of the inertia tensor, we distinguish asteroids in a long-axis mode (LAM) and short-axis mode (SAM) of rotation. In the case of SAM or LAM tumblers, an asteroid rotates around its shortest or longest axis (Kaasalainen, 2001).

There are several ways an asteroid can become a tumbler. In general, the asteroid must change the direction of its angular momentum vector. One such process is the YORP effect[3], where solar radiation impacts the asteroid's rotation. In simple terms, an asteroid absorbs solar energy and reemits it as thermal radiation, but with a time lag. Depending on the asteroid's axis inclination and shape, this effect can gradually alter its angular momentum vector. Over long periods, these dynamical changes can modify the asteroid's rotational state. It is important to note that the shape of the asteroid also plays a crucial role, as specific shapes are more susceptible to this effect than others (Vokrouhlický et al., 2015). Another way an asteroid can become a tumbler is through a collision with another body.

3. Yarkovsky–O'Keefe–Radzievskii–Paddack effect

1 Lightcurves of tumblers

Photometry is the only way to obtain information about an asteroid's rotational state. A photometric measurement yields a light curve, which shows the light flux as a function of time.

In the case of normal asteroids, rotating around the principal axis, light curves are modeled by the single-period Fourier series

$$F(t) = C_0 + \sum_{n=1}^{m} C_n \cos\left(\frac{2\pi n}{P} t\right) + \sum_{n=1}^{m} S_n \sin\left(\frac{2\pi n}{P} t\right), \tag{1.1}$$

where P is the period, C_n, S_n are the Fourier coefficients and m is the order of the Fourier series. Fourier series can be rewritten in the phase form

$$F(t) = C_0 + \sum_{n=1}^{m} A_n \cos\left(\frac{2\pi n}{P} t - \varphi_n\right), \tag{1.2}$$

where $A_n = \sqrt{C_n^2 + S_n^2}$ and $\varphi_n = \arctan 2(S_n, C_n)$.

In the case of tumblers, there are two physical periods: one related to rotation and one related to precession. The source of both periods is one body, which means it is impossible to separate the periods. A two-dimensional Fourier series model of the light curve of the tumbler is

$$\begin{aligned} F(\psi(t), \phi(t)) \doteq F^m(t) = C_0 &+ \sum_{j=1}^{m} \left[C_{j0} \cos\left(\frac{2\pi j}{P_\psi} t\right) + S_{j0} \sin\left(\frac{2\pi j}{P_\psi} t\right) \right] \\ &+ \sum_{k=1}^{m} \sum_{j=-m}^{m} \left[C_{jk} \cos\left(\frac{2\pi j}{P_\psi} + \frac{2\pi k}{P_\phi}\right) t \right. \\ &+ \left. S_{jk} \sin\left(\frac{2\pi j}{P_\psi} + \frac{2\pi k}{P_\phi}\right) t \right], \end{aligned} \tag{1.3}$$

where P_ψ and P_ϕ are the periods of the tumbler (rotation and precession) and m is the order of the Fourier series (Pravec et al., 2005). Fourier series for tumbling asteroids can also be rewritten to phase form similarly as for a PA rotator

$$F(\psi(t), \phi(t)) \doteq F^m(t) = C_0 + \sum_{j=1}^{m} A_{j0} \cos\left(\frac{2\pi j}{P_\psi} t - \varphi_{j0}\right) + \sum_{k=1}^{m} \sum_{j=-m}^{m} A_{jk} \cos\left[\left(\frac{2\pi j}{P_\psi} + \frac{2\pi k}{P_\phi}\right) t - \varphi_{jk}\right], \tag{1.4}$$

where $A_{jk} = \sqrt{C_{jk}^2 + S_{jk}^2}$ and $\varphi_{jk} = \arctan 2(S_{jk}, C_{jk})$.

The most widely used is the notation P_1 and P_2 rather than P_ψ and P_ϕ because, in most cases, we cannot directly say which period is precession and which is rotation. In this thesis, we will rather use frequencies $f = \frac{1}{P}$ instead of the periods. In case of tumblers, coefficients C_{jk} and S_{jk} correspond with frequency $f_{jk} = jf_1 + kf_2$.

1.1 Frequencies in the light curve

Usually, the highest peaks in the power spectrum of the light curve are not the real frequencies ($f_\psi = P_\psi^{-1}$ and $f_\phi = P_\phi^{-1}$), but rather their linear combinations.

Asteroids rotate in two modes, LAM and SAM. Because of this, we can use two conventions, L-convention and S-convention, for the description of the rotating bodies. The convention used mainly is S (usually denoted by the subscript S (P_{ψ_S}, P_{ϕ_S}))(Samarasinha and Mueller, 2015).

There are some connections between the frequencies of different conventions and different modes. For all tumblers, we can write the connection between the rotation periods in the L and S convention as

$$f_{\psi_L} = f_{\psi_S}\,. \tag{1.5}$$

For the precession periods, we cannot write this simple equation because it also depends on rotation by

$$f_{\phi_S} = f_{\phi_L} + f_{\psi_L}\,. \tag{1.6}$$

We can directly see the information about precession periods $f_{\phi_S} > f_{\phi_L}$. (Samarasinha and Mueller, 2015).

In most cases, the two prominent periods are $2f_{\phi_\mathrm{L}}$ and $2f_{\phi_\mathrm{S}}$[4] (Samarasinha and Mueller, 2015;Kaasalainen, 2001). Other dominant frequencies in the light curves can be $1f_{\phi_\mathrm{L}}$, $1f_{\phi_\mathrm{S}}$ or $1f_{\phi_\mathrm{L}} + 2f_{\psi_\mathrm{L}}$ ($1f_{\phi_\mathrm{S}} + 1f_{\psi_\mathrm{S}}$), or the frequencies directly connected to the rotational frequency, f_ψ (Samarasinha and Mueller, 2015).

4. For conversion of the precession frequency from one convention to another we can use equation 1.6 and equation $f_{\phi_\mathrm{L}} = f_{\phi_\mathrm{S}} - f_{\psi_\mathrm{S}}$, which is derived from equations 1.6 and 1.5.

2 Fourier transform

Fourier analysis is a useful technique for analyzing periodic functions. This technique decomposes the periodic function as a time series into simple sinusoidal waves, transforming the function from the time domain to the frequency domain.

The equation defines the Fourier transform (FT) from the time to the frequency domain

$$F(\nu) = \mathcal{F}\{f(t)\} = \int_{-\infty}^{\infty} f(t)e^{-2\pi i\nu t}dt\,, \tag{2.1}$$

where $f(t)$ is a function in time domain, t is time and ν is frequency. The inverse Fourier transform is given by the equation

$$f(t) = \mathcal{F}^{-1}\{F(\nu)\} = \int_{-\infty}^{\infty} F(\nu)e^{2\pi i\nu t}d\nu\,. \tag{2.2}$$

For the function in the time domain and its representation in the frequency domain, we can write Rayleigh's theorem

$$\int_{-\infty}^{\infty} |f(t)|^2\,dt = \int_{-\infty}^{\infty} |F(\nu)|^2\,d\nu\,, \tag{2.3}$$

where

$$P(\nu) = |F(\nu)|^2 = \left|\int_{-\infty}^{\infty} f(t)e^{-2\pi i\nu t}dt\right|^2\,, \tag{2.4}$$

is the power spectrum and for the real function $f(t)$, the function $F(\nu)$ satisfies $F(-\nu) = F^*(\nu)$ (Roberts et al., 1987), where F^* means complex conjugated function. Two functions $F(\nu)$ and $f(t)$ are usually called Fourier pair. The most important Fourier pair is a sinusoid with frequency f_0 and two delta functions at frequencies $\pm f_0$ ($\mathcal{F}\{\cos 2\pi f_0 t\} = \frac{1}{2}[\delta(f-f_0)+\delta(f+f_0)]$).

The Fourier transform has several useful properties. FT is linear, so that we can write for any constant A, and any two functions $f(x)$ and $g(x)$

$$\mathcal{F}\{f(x)+g(x)\} = \mathcal{F}\{f(x)\} + \mathcal{F}\{g(x)\}\,, \tag{2.5}$$

$$\mathcal{F}\{Af(x)\} = A\,\mathcal{F}\{f(x)\}\,. \tag{2.6}$$

The second important property is that the time shift impacts only the phase, not the amplitude

$$\mathcal{F}\{g(t-t_0)\} = \mathcal{F}\{g(t)\}e^{-2\pi i f t_0}\,. \tag{2.7}$$

2.1 Real (sampled) data

In reality we do not observe continuous function f but the set of discrete points $\{f_r, t_r\} \equiv \{f(t_r), t_r\}$. These points are given by a real periodic function of physical phenomena $f(t)$ and sampling function

$$s(t) = \frac{1}{N}\sum_{r=1}^{N}\delta(t-t_r)\,. \tag{2.8}$$

The sampled signal is now given by the product of these two functions

$$f_{\mathrm{s}}(t) \equiv f(t)s(t) = \frac{1}{N}\sum_{r=1}^{N} f_r\delta(t-t_r)\,. \tag{2.9}$$

By the Fourier transformation of the sampled signal we get the "dirty spectrum"

$$D(\nu) = \mathcal{F}\{f_{\mathrm{s}}\} = \mathcal{F}\{f(t)\cdot s(t)\}\,, \tag{2.10}$$

which can be rewritten by the convolution

$$D(\nu) = F(\nu) \circledast W(\nu) \tag{2.11}$$

where $F(\nu) = \mathcal{F}\{f(t)\}$ and $W(\nu) = \mathcal{F}\{s(t)\}$. By the definition of the Fourier transform (equation 2.1), we get the Fourier transform of the dirty spectrum

$$D(\nu) = \int_{-\infty}^{\infty} f_s(t)e^{-2\pi i\nu t}dt\,. \tag{2.12}$$

For the discrete data, this integral collapses to the discrete Fourier transform

$$D(\nu) = \frac{1}{N}\sum_{r=1}^{N} f_r e^{-2\pi i\nu t_r}\,. \tag{2.13}$$

For the discrete data, the periodogram equation 2.4 collapses to a periodogram for discrete data

$$P(\nu) = |F(\nu)|^2 = \frac{1}{N}\left|\sum_{r=1}^{N} f_r e^{-2\pi i \nu t_r}\right|^2 , \tag{2.14}$$

Analogously, we get the definition of the Fourier transform for the window

$$W(\nu) = \int_{-\infty}^{\infty} s(t) e^{-2\pi i \nu t} dt \tag{2.15}$$

and rewritten to a discrete form

$$W(\nu) = \frac{1}{N}\sum_{r=1}^{N} e^{-2\pi i \nu t_r} . \tag{2.16}$$

The window function, or spectral window, is the Fourier transform of the sampling function $s(t)$. Spectral window captures effects of irregular and finite sampling.

For dirty spectrum and window, we get the same identities as for the F: $D(-\nu) = D^*(\nu)$, $W(-\nu) = W^*(\nu)$. It is seen that the real periodogram as a solution of equation 2.11 is

$$F(\nu) = \mathcal{F}\{f\} = \mathcal{F}\{f_s/s\} = \mathcal{F}\{f_s\} \circledast \mathcal{F}\{1/s\} . \tag{2.17}$$

The complication is that this equation has no unique solution because no finite set of data points can fully specify the function $f(t)$ (Roberts et al., 1987). The next consequence of discrete sampling is that we cannot derive any frequency, but Nyquist's theorem limits us (Press, 2007). When we define $f_s = 1/\Delta$ as sampling frequency, where Δ is sampling interval, we get Nyquist's critical frequency as

$$f_c = \frac{1}{2} f_s = \frac{1}{2\Delta} . \tag{2.18}$$

This frequency is the limit in the frequency calculation and represents the highest frequency that can be derived (Press, 2007). For non-uniformly sampled data, we use $\Delta_{\min}$ as the sampling interval, which is the smallest distance between any two data points.

2.1.1 Dirty and Clean spectrum

Due to the impossibility of uniquely deconvolving dirty spectra, various methods have been developed to address this challenge. One of them is the CLEAN algorithm (Roberts et al., 1987). Initially developed in the context of radio astronomy, the CLEAN algorithm has been adapted for spectral analysis to remove spurious features caused by the spectral window function through an iterative process. The main idea is to isolate the main peaks, subtract them and their features from the dirty spectrum, and create a clean spectrum.

The CLEAN algorithm (Roberts et al., 1987) produces the residual spectrum and subtracts the main peak from it. We start with notation $R^0 = D$. Next, we start iterations.

1. Find the main (the highest) peak on frequency ν^i and calculate the amplitude of the clean component $c^i = g\alpha(R^{i-1}, \nu^i)$, where g is the gain. Gain is a parameter of the CLEAN algorithm used for moderation, mostly set to 0.5, but any value in the range $(0, 2)$ should converge to the solution. α is given by the equation

$$\alpha(D, \nu) = \frac{D(\nu) - D^*(\nu)W(2\nu)}{1 - |W(2\nu)|^2} \,. \tag{2.19}$$

2. Form the new residual spectrum by subtracting the found peak

$$R^i(\nu) = R^{i-1}(\nu) - (c^i W(\nu - \nu^i) + (c^i)^* W(\nu + \nu^i)) \,. \tag{2.20}$$

3. Control if residual spectrum or accumulated components achieve some stopping condition. If not, repeat steps 1, 2, and 3; if so, proceed to step 4.

4. Fit the clean beam B to the window function W and construct the clean spectrum defined as

$$S(\nu) = \sum_{i=1}^{K} (c^i B(\nu - \nu^i) + (c^i)^* B(\nu + \nu^i)) + R^K(\nu) \,. \tag{2.21}$$

The stopping condition mentioned in step 3 is typically related to the residual spectrum, and the algorithm is stopped when the residual spectrum is essentially noise. This indicates that the dominant frequency components have been successfully removed from the data, and further iterations would not yield meaningful improvements. To ensure that CLEAN works correctly, the window function must be computed over the frequency range $(-2\nu_{\max}, 2\nu_{\max})$ to have window in $(-\nu_{\max}, \nu_{\max})$ (Roberts et al., 1987).

2.2 Lomb-Scargle periodogram

Lomb-Scargle (LS) periodogram is a general method to find the periodogram in various time series. The LS periodogram is primarily used for unevenly sampled time series. It was first published in papers Lomb, 1976 and Scargle, 1982. Astronomy time series are typically unevenly sampled due to weather conditions and Earth's rotational and orbital movements.

In Scargle, 1982, this periodogram was rewritten into trigonometric form and three arbitrary functions A, B, and τ were added

$$P(\nu) = \frac{A^2}{2}\left(\sum_n f_n \cos\left(2\pi\nu(t_n - \tau)\right)\right)^2 \tag{2.22}$$

$$+ \frac{B^2}{2}\left(\sum_n f_n \sin\left(2\pi\nu(t_n - \tau)\right)\right)^2, \tag{2.23}$$

where A,B and τ are arbitrary functions of frequency ν and time t_n. For unique values of A and B periodogram leads to a general form of the Lomb-Scargle periodogram

$$P_{\mathrm{LS}}(\nu) = \frac{1}{2}\left\{ \left(\sum_n f_n \cos(2\pi\nu[t_n - \tau])\right)^2 \Big/ \sum_n \cos^2(2\pi\nu(t_n - \tau)) + \left(\sum_n f_n \sin(2\pi\nu[t_n - \tau])\right)^2 \Big/ \sum_n \sin^2(2\pi\nu(t_n - \tau)) \right\}, \tag{2.24}$$

where τ is specified to ensure time-shift invariance

$$\tau = \frac{1}{4\pi\nu} \tan^{-1}\left(\frac{\sum_n \sin\left(4\pi\nu t_n\right)}{\sum_n \cos\left(4\pi\nu t_n\right)}\right). \tag{2.25}$$

The difference between this version of the modified periodogram and the classical one depends on the difference between denominators $\sum_n \cos^2(2\pi\nu(t_n))$ and $\sum_n \sin^2(2\pi\nu(t_n))$ from $N/2$ (VanderPlas, 2018).

3 Genetic algorithms

A genetic algorithm is a numerical method suitable for optimizing problems. The genetic algorithm works through a few simple steps. Firstly, it randomly generates a zero population. Next, it evaluates individuals based on the defined fitness function. Then, it selects individuals with a higher fitness value, executes a crossover and a mutation to produce a new generation. These steps are repeated until the stopping condition is satisfied. The scheme of the genetic algorithm is shown in Figure 3.1 (Buranský, 2023).

3.1 Genome structure and evolution operators

In this thesis, I used real-valued encoding, which means that a candidate for a solution is a vector of real numbers, and each number is a free parameter (Blanco et al., 2001). I stacked all parameters into a vector and used an assistant function to decompose this vector into individual model parameters.

3.1.1 Operators

There are two operators, crossover and selection, which converge to the extreme of the fitness function, and one operator, mutation, which allows escape from the local extremes.

The main operator for changing the genome is **crossover**. Crossover takes two parents (vectors) and produces a new array using the equation[5]

$$o_n = \alpha_n \odot p_{1_n} + (1 - \alpha_n) \odot p_{2_n} \,, \tag{3.1}$$

where o is offspring, p_1 and p_2 are the parents, and α is the vector of the same length as the parents, containing numbers in the interval $[0, 1]$. Crossover is not performed in all cases, but we use the probability of crossover to achieve fast convergence; this probability is typically higher than 90%.

5. Symbol $\odot$ stands for the Hadamard product. This product is defined as $(\mathbf{A} \odot \mathbf{B})_{ij} = \mathbf{A}_{ij} \cdot \mathbf{B}_{ij}$. (Chakrabarty, 2015).

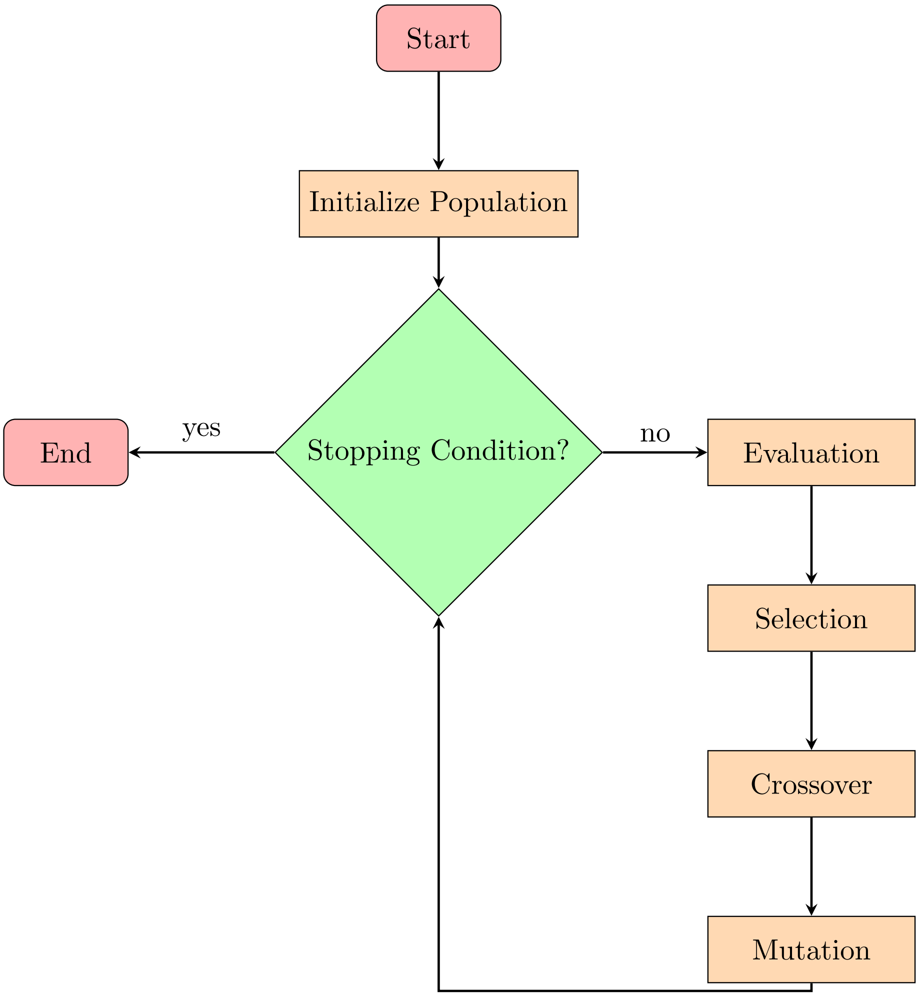

Figure 3.1: Scheme of the genetic algorithm.

Mutation is the operator for the small changes in the genome and is needed to escape from the local extremes of the fitness function. The equation gives a mutation for real-value encoding

$$o'_n = o_n + \beta_n \,, \tag{3.2}$$

where o is offspring, o' is the mutated offspring, and β is a vector that contains random numbers in a given range. Usually, almost all elements in vector β are zero due to the probability of mutation. The probability of mutation is usually a few percent or sometimes less than one percent. For better convergence, the **adaptive mutation** is sometimes used. Adaptive mutation is a technique used to better escape from local minima when the population is stuck for more generations.

Example

Crossover:

$$\mathbf{o} = \boldsymbol{\alpha} \odot \mathbf{p}_1 + (1 - \boldsymbol{\alpha}) \odot \mathbf{p}_2$$

$$\boldsymbol{\alpha} = \begin{bmatrix} 0.2 \\ 0.5 \\ 0.8 \end{bmatrix} \quad \mathbf{p}_1 = \begin{bmatrix} 1 \\ 2 \\ 3 \end{bmatrix} \quad \mathbf{p}_2 = \begin{bmatrix} 4 \\ 5 \\ 6 \end{bmatrix}$$

$$\mathbf{o} = \begin{bmatrix} 0.2 \cdot 1 + 0.8 \cdot 4 \\ 0.5 \cdot 2 + 0.5 \cdot 5 \\ 0.8 \cdot 3 + 0.2 \cdot 6 \end{bmatrix} = \begin{bmatrix} 3.4 \\ 3.5 \\ 3.6 \end{bmatrix}$$

Mutation:

$$\boldsymbol{\beta} = \begin{bmatrix} 0.00 \\ +0.02 \\ 0.00 \end{bmatrix} \quad \mathbf{o}' = \mathbf{o} + \boldsymbol{\beta} = \begin{bmatrix} 3.40 \\ 3.52 \\ 3.60 \end{bmatrix}$$

Fitness Proportional Selection, also known as **Roulette Wheel Selection**, is the most common and famous selection method in genetic algorithms. In this method, the parents for crossover are selected randomly, but the probabilities of being selected are given by the equation

$$p_i = \frac{f_i}{\sum_{i=1}^{n} f_i} \,, \tag{3.3}$$

where f_i is the fitness function and n is the size of the population (Jebari, Madiafi, et al., 2013). **Tournament Selection** takes a smaller part of the population (tournament) and selects the best individual as the winner. The tournament is done n times to fill the next population (Jebari, Madiafi, et al., 2013). **Rank Based Selection** is similar to fitness-proportional selection. The fitness function values sort the individuals in the population in ascending order, and each individual is given a rank. The equation gives the probability of being selected (Jebari, Madiafi, et al., 2013)

$$p_i = \frac{i}{\sum_{i=1}^{n} i} \,. \tag{3.4}$$

Elitism Selection is a method for faster convergence and no loss of best individuals. It means that the time evolution of the fitness function of the best individual will be a non-decreasing function. It is done by taking the first few best individuals and simply copying them to the next generation without any changes (Du et al., 2018).

3.2 Fitness function

The most important part of the genetic algorithm is the fitness function. The fitness function defines a problem and selects better and worse solutions. In the genetic algorithm process, the fitness function is connected with the probability of an individual being selected, meaning it must have only positive values.

The suitable fitness function for the fitting of the data is χ^2, which is defined as

$$\chi^2 = \sum_{i=0}^{N-1} \left(\frac{y_i - y\left(x_i | a_0, ..., a_{M-1}\right)}{\sigma_i} \right)^2 , \tag{3.5}$$

where N is the number of data points, $[x_i, y_i]$ are the data points, σ_i are uncertainties of the y_i and $(a_0, ..., a_{M-1})$ are the free parameters (M is the number of the free parameters). For the "moderately" good fit χ^2 can be approximated as

$$\chi^2 \approx \nu = N - M \,, \tag{3.6}$$

where ν is the number of degrees of freedom (Press, 2007).

For the genetic algorithm usage, we need to have an increasing fitness function (because in almost every case of genetic algorithm, fitness function directly means the probability to be selected), so we use inverted χ^2 as fitness function

$$''\text{fitness}'' = \frac{1}{\chi^2} \approx \frac{1}{\nu}\,. \tag{3.7}$$

3.3 The stopping criterion

The persistent challenge is determining when to stop the genetic algorithm's run. Typical methods stop after several generations or when the fitness function reaches a threshold. The problem is that we do not know the sufficient number of generations to reach a good solution. Usually, the same problem is with the fitness threshold. In some cases, we can use the information from equation 3.6, that χ^2 is approximately equal to the number of degrees of freedom.

4 Methods of analyzing light curves

In this thesis, I implement and test different methods to analyze light curves of tumbling asteroids. The project and tests are in the GitHub repository (Appendix A). I tested different synthetic light curves of various asteroids, which have varying numbers of data points, uncertainties, and breaks, simulating real observations. These results are in section 4.3 for PA rotating asteroids and in Chapter 5 for NPA rotating asteroids (tumblers).

4.1 Clean Fourier periodogram and Lomb-Scargle periodogram

The first method is the Fourier periodogram, described theoretically in Section 2.1. First, I calculate the frequency grid with m positive frequency points. When we calculate just positive frequency (due to the symmetry of the Fourier periodogram), the frequency grid is given by the equation

$$\nu_j = \frac{j}{m}\nu_{\max}\,, \tag{4.1}$$

where $j = 0, \ldots, m$ and $\nu_{\max}$ is the maximum frequency that we can detect from data, and Nyquist's theorem gives it as

$$\nu_{\max} = \frac{1}{2\Delta_{\min}}\,, \tag{4.2}$$

where $\Delta_{\min}$ is the minimal time distance between two points in the light curve and m is given as

$$m = n_{\mathrm{B}}\left(\frac{\nu_{\max}}{\delta_\nu}\right)\,, \tag{4.3}$$

where $\delta_\nu \approx \frac{1}{T}$, so we can write

$$m = n_{\mathrm{B}}\left(\frac{T}{2\Delta_{\min}}\right)\,, \tag{4.4}$$

where T is the time length of the light curve. Finally, the parameter n_{B} is the number of "points per beam" and it controls the periodogram's accuracy. The typical value is $n_{\mathrm{B}} = 4$ and higher (Roberts et al., 1987).

On this frequency grid, I calculate the value of the Fourier transformed function by the definition (equation 2.13) of the unevenly sampled data. Finally, I used the CLEAN algorithm described in Section 2.1.1.

In this thesis, I also use and analyze the Lomb-Scargle periodogram of the given light curves. In the Lomb-Scargle periodogram, I search for indications of aliasing. After this, it is necessary to find out which frequencies are aliases. I verify whether another peak exists at approximately twice or three times the frequency of the current peak. This helps to identify harmonic relationships between peaks. I also check whether there is a peak that appears at a frequency shifted from the current peak by a known offset introduced by the window function. This helps detect artifacts such as spectral leakage or side lobes.

4.2 Genetic algorithm

Finally, once we get the results from the Lomb-Scargle periodogram (or CLEAN Fourier periodogram) and want to do a precise fit. We employ the genetic algorithm (described in Chapter 3). The results of the Fourier periodogram (or Lomb-Scargle periodogram) provide good starting parameters for the genetic algorithm. The genetic algorithm is a robust numerical method, but it should work better and faster with a smaller parameter space.

In most cases, dominant frequencies in the periodogram do not have to be rotational and precessional (more in Section 1.1). This means that we cannot be certain we have found the physical frequencies; we can only find frequencies f_1 and f_2, which should be proven by another method. In some cases, we can find clues in peaks. The most dominant frequencies are usually f_{ϕ_L}, f_{ϕ_S}, their doubles and f_ψ and its multiples. The frequency and its double in the periodogram can also serve as well, which is also the case when the sum of two frequencies is present in the periodogram. In the thesis, the first estimation from the periodogram is used to set a smaller interval for the genetic algorithm to find frequencies.

According to the principles of genetic algorithms (random operators selection, crossover, and mutation involve elements of chance), which inherently rely on stochastic or random processes, the outcomes of each run can vary slightly. Results can also differ when GA has the same initial conditions on the same problems. As a result, a single run of the algorithm may not provide a fully reliable or representative solution. To improve the precision and reliability of the results, it is recommended to run the genetic algorithm multiple times under the same conditions on the same problem. By doing so, it is possible to collect a distribution of results, which allows for statistical analysis, such as computing averages[6]. However, for such statistical evaluation to be meaningful, it is crucial to ensure consistency across all runs, including the same search parameter space, number of individuals, and order of the Fourier series.

4.3 Testing methods on PA rotator

To better understand and test the presented methods, we apply them to the computer-generated data of the principal axis rotators (PA rotator, an asteroid rotating around the principal axis with a single period in its light curve).

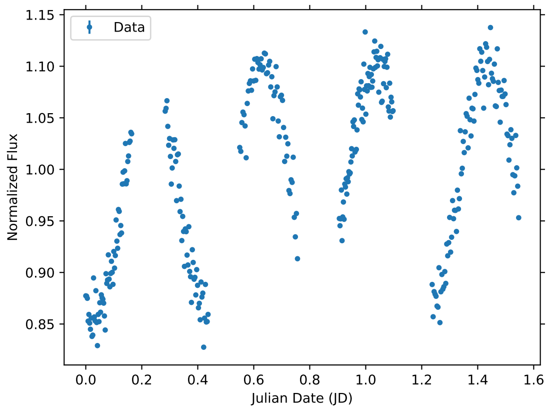

Figure 4.1: PA rotator synthetic data (ID1925).

6. The mean value, $\bar{x}$, and its error, σ_{M}, are given as (Moore et al., 2016) $\bar{x} = \frac{1}{n}\sum_{i=1}^{n} x_i$, and $\sigma_{\mathrm{M}} = \sqrt{\frac{\sum_{i=1}^{n}(x_i-\bar{x})^2}{n(n-1)}}$, where x_i is the i-th value, n is the size of the data. Results can be written as $\bar{x} \pm \sigma_{\mathrm{M}}$.

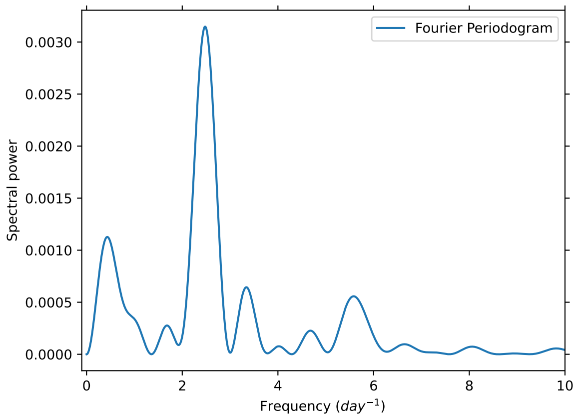

Figure 4.2: Fourier periodogram (ID1925).

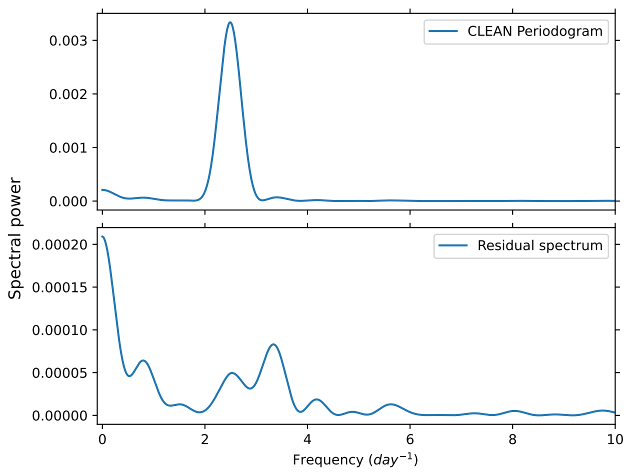

Figure 4.3: Clean Fourier periodogram (ID1925). The most dominant peak is on frequency $2.4962\,\mathrm{d}^{-1}$.

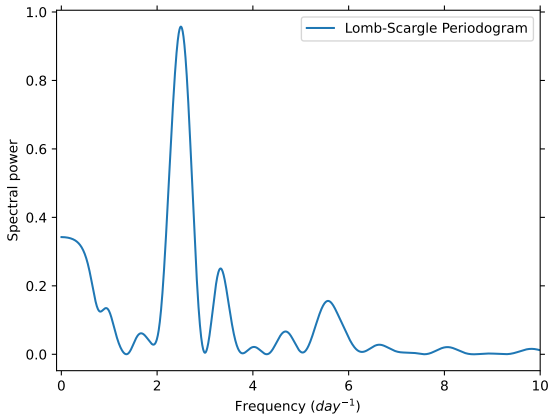

Figure 4.4: Lomb-Scargle periodogram (ID1925). The most dominant peak occurs at a frequency $2.5221\,\mathrm{d}^{-1}$. The most dominant frequency in the Spectral window is $3.1946\,\mathrm{d}^{-1}$.

The Fourier periodogram and CLEAN Fourier periodogram clearly show that the main (and only) peak is around frequency $2.4962\,\mathrm{d}^{-1}$ or $2.5221\,\mathrm{d}^{-1}$ in the Lomb-Scargle periodogram. Now, to achieve results, we make the fit using the genetic algorithm, with a good first estimate of the frequency.

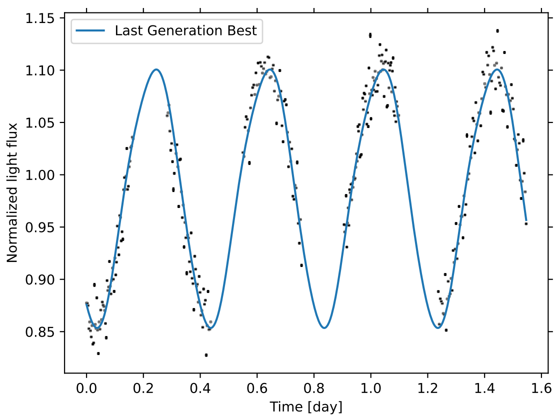

Figure 4.5: Fit by genetic algorithm of light curve ID1925.

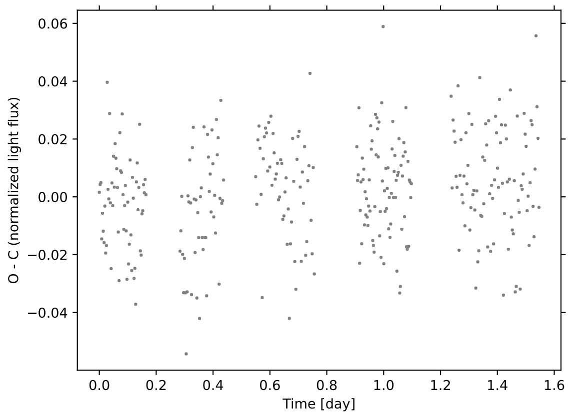

Figure 4.6: $O - C$ graph of genetic algorithm fit of light curve ID1925.

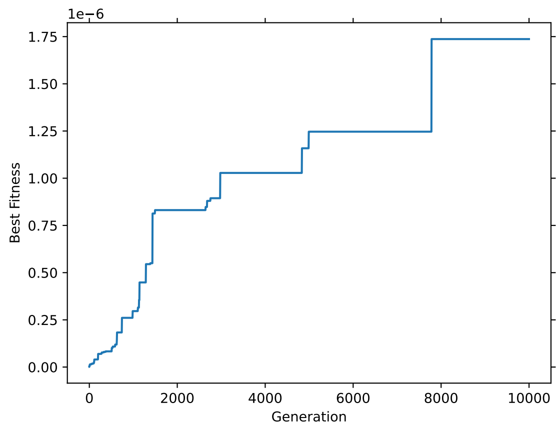

Figure 4.7: Fitness evolution of genetic algorithm fit of light curve ID1925.

Table 4.1: Parameters of genetic algorithm fit of light curve ID1925.

Number of individuals	250	
Number of generations	10 000	
Order of Fourier series	3	
Number of data points	335	
χ^2	576 000	
	Calculated	Real
Frequency f[day^{-1}]	2.50	1.25
Period P[hours]	9.60	19.23

4.4 Discussion

In this part, I applied all the described methods on the light curve of the PA rotator (ID1925). In the periodograms, I obtain a single dominant peak at frequency $f \approx 2.50\,\mathrm{d}^{-1}$. Next, I used a genetic algorithm to fit the light curve, and as an estimate, I used the periodogram to determine the frequency. From the fit, I obtain almost the same frequency and rotational period of the asteroid as $P = 9.60\,\mathrm{h}$. The true period is 19.23 h, which is nearly double that of my calculated rotational period.

The reason is that the simulated rotation of a triaxial ellipsoid generated our data. The light curve generated through this process has identical minimas and identical maximas because the opposing sides of the asteroid are also similar. In a real asteroid's light curve, the neighbouring minima (or maxima) differ according to their irregular shape.

5 Analysing data of tumbling asteroids

5.1 Data

For this thesis, I used computer-generated data that simulated the real observations. In real-world observations, we have gaps due to daylight or weather conditions. In real data sets, we sometimes take observations from several telescopes and create a light curve. Each telescope observes with its particular sampling, meaning we have some random sampling in the final light curve. This section shows several light curves, each exhibiting distinct temporal and sampling characteristics. In the next parts, data is analyzed as described in Chapter 4.

Next, there are three light curves ID1916, ID1917, and ID1916_long (Appendix B). All of them are light curves of the same body. Light curves and their analysis of the different bodies are shown in Appendix C.

The data used has a different parameter σ, which is defined as $\sigma = s \cdot \Delta_{\text{flux}}$, where Δ_{flux} is the difference between maximal and minimal flux in the light curve.

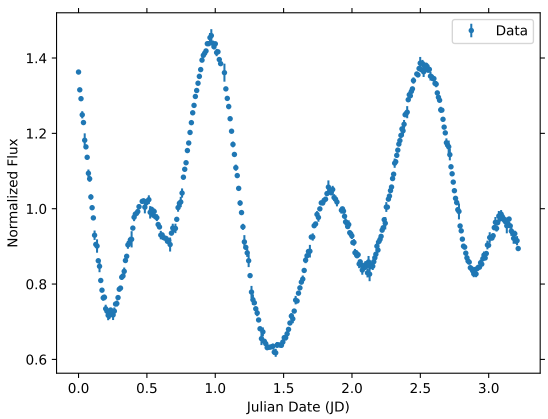

Figure 5.1: Synthetic tumbler light curve ID1916 with standard deviation $s = 0.01$. The other two light curves of the same tumbler are in Appendix B.

5.2 Results

5.2.1 Fourier periodogram

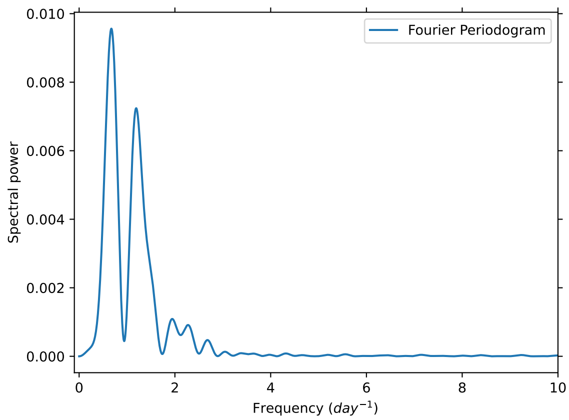

Figure 5.2: Fourier periodogram of light curve ID1916 with $s = 0.01$.

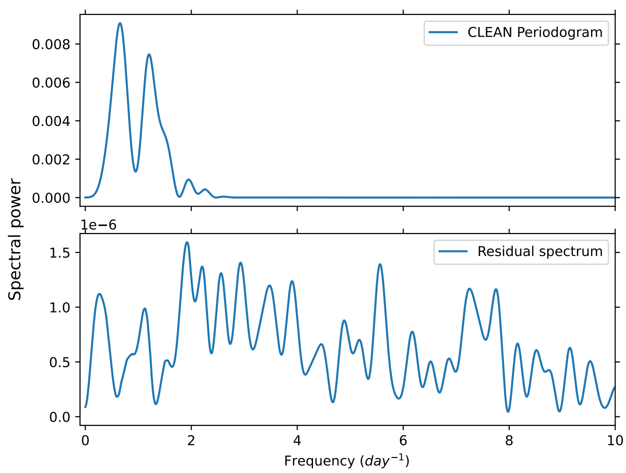

Figure 5.3: Clean Fourier periodogram of light curve ID1916 with $s = 0.01$. The most dominant peaks are on frequencies $0.6546\,\mathrm{d}^{-1}$ and $1.2034\,\mathrm{d}^{-1}$. CLEAN periodograms of the two other light curves of the same tumbler are in Appendix B.

5.2.2 Lomb-Scargle periodogram

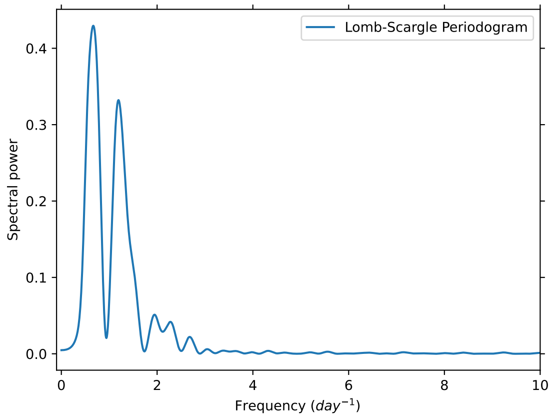

Figure 5.4: Lomb-Scargle periodogram of light curve ID1916 with $s = 0.01$. The most dominant peaks are on frequencies $0.6670\,\mathrm{d}^{-1}$ and $1.1925\,\mathrm{d}^{-1}$. The dominant peak in the Spectral window is at a frequency $0.4509\,\mathrm{d}^{-1}$. Lomb-Scargle periodograms of the two other light curves of the same tumbler are in Appendix B.

In all three light curves, the most dominant peaks are around $0.65\,\mathrm{d}^{-1}$, $1.10\,\mathrm{d}^{-1}$, $0.75\,\mathrm{d}^{-1}$, $1.20\,\mathrm{d}^{-1}$. The peak $0.75\,\mathrm{d}^{-1}$ is the only one that has higher frequencies ($1.5\,\mathrm{d}^{-1}$, $2.25\,\mathrm{d}^{-1}\ldots$) in all periodograms. We can assume that this is the frequency f_1 (probable rotational). One higher peak should be precession in S-convention and one smaller peak in L-convention. These frequencies fulfill the equation 1.6. The frequency around $0.65\,\mathrm{d}^{-1}$ can be double that of the precession in L-convention. It is supported by half of this frequency around $0.33\,\mathrm{d}^{-1}$. The sum of precession in L-convention and rotation frequencies is precession in S-convention. A peak around $1.10\,\mathrm{d}^{-1}$ is visible in periodograms.

It is probable that searching frequencies of this body are $f_1 \approx 0.35\,\mathrm{d}^{-1}$ and $f_2 \approx 0.75\,\mathrm{d}^{-1}$. This is merely the best final suggestion. I also had various incorrectly guessed frequencies, either higher or lower, and the final suggestion converges to a relatively good fit by the genetic algorithm. It was visible at the end of the light curve that the frequencies are inaccurate (higher or lower).

5.2.3 Genetic algorithm

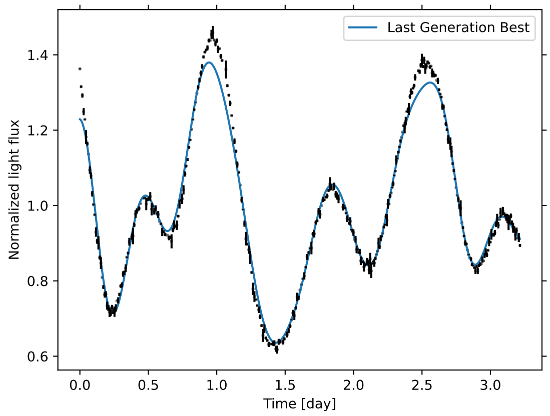

Figure 5.5: Fit by genetic algorithm of light curve ID1916 with $s = 0.01$

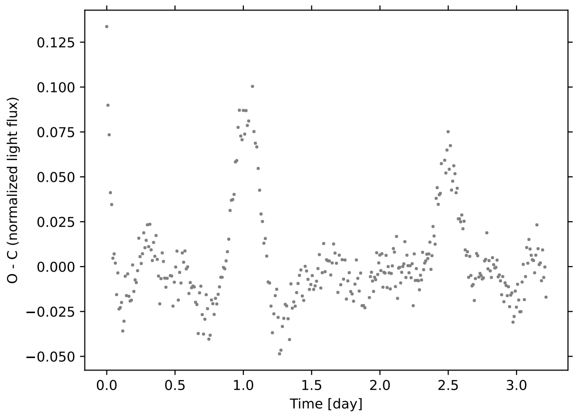

Figure 5.6: $O - C$ graph of genetic algorithm fit of light curve ID1916 with $s = 0.01$

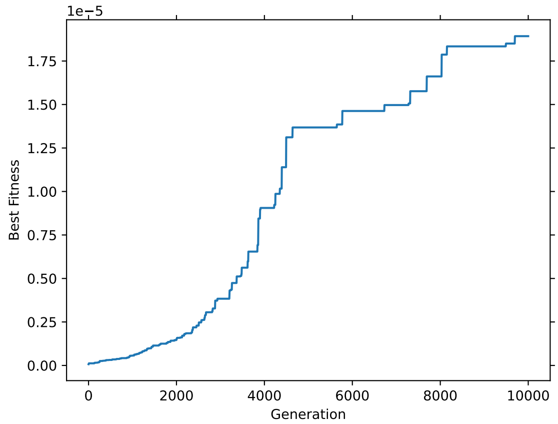

Figure 5.7: Fitness evolution of genetic algorithm fit of light curve ID1916 with $s = 0.01$

Table 5.1: Parameters of genetic algorithm fit of light curve ID1916 with $s = 0.01$.

Number of individuals	300	
Number of generations	20 000	
Order of Fourier series	3	
Number of data points	350	
χ^2	52 800	
	Calculated	Real
Frequency $f_1\,[\text{day}^{-1}]$	0.7691	0.7689
Frequency $f_2\,[\text{day}^{-1}]$	0.3302	0.3286
Period $P_1\,[\text{hours}]$	31.2053	31.2134
Period $P_2\,[\text{hours}]$	72.6832	73.0478

6 Disccusion

In Chapter 5, synthetic light curves were used to determine which frequencies (periods) manifest most in different cases of asteroid rotation and how to find them.

6.1 ID1916, ID1917, ID1916_long

First, I tested the three light curves of the same tumbler (ID1916, ID1917, and ID1916_long). From periodograms of these three light curves of the same body, we obtain an approximation of this body's rotational and precessional frequencies. The genetic algorithm fit tested the guess. The periods from the rotation are $P_1 = 31.2053\,\mathrm{h}$ and $P_2 = 72.6832\,\mathrm{h}$. The real periods used in the creation of the synthetic data were $P_\psi = 31.2134\,\mathrm{h}$ and $P_\phi = 73.0478\,\mathrm{h}$. The differences are 0.03% for the rotation and 0.5% for the precession.

In these three light curves, we can see that each periodogram has different frequency peaks despite the three light curves being from the same body. First, with the longer light curve, we detect more frequencies.

6.2 ID1913, ID1915

The second tested light curve was ID1913 (and ID1915, which is the same but with gaps representing nighttime observations). These light curves differ from others because of the extended observation period. Due to this, we can see that more peaks and more frequencies are present in both periodograms. There is also the third for the first two peaks, which is their sum. This indicates that these three peaks are precession in L-convention, rotation, and precession in S-convention.

In the periodogram of the light curve ID1915, aliasing is visible as indicated by the strictly daytime observation. In the spectral window, the strongest peak is around $f = 1.00\,\mathrm{d}^{-1}$. In the light curve periodogram, we can find the pairs of the frequency - one at the proper frequency and another shifted by approximately $1.00\,\mathrm{d}^{-1}$

e.g. ($0.3243\,\mathrm{d}^{-1}$;$1.3499\,\mathrm{d}^{-1}$), ($0.6633\,\mathrm{d}^{-1}$; $1.6631\,\mathrm{d}^{-1}$) or ($0.9756\,\mathrm{d}^{-1}$; $1.9701\,\mathrm{d}^{-1}$).

The periods found by the genetic algorithm in the light curve ID1913 are $P_1 = 35.2786\,\mathrm{h}$ and $P_2 = 74.7431\,\mathrm{h}$ and the real ones are $P_\psi = 34.4135\,\mathrm{h}$ and $P_\phi = 80.5639\,\mathrm{h}$. The differences are 7% and 3%. This light curve is longer (with more data points), but there is evident higher noise in the data, which can cause a larger discrepancy between the calculated frequencies and the actual ones.

6.3 ID1918

I found no clues about multiple frequencies or the sum of the frequencies in the periodogram of the light curve ID1918. Frequencies found by periodograms and genetic algorithm fit are $f_1 = 0.3313\,\mathrm{d}^{-1}$ and $f_2 = 0.6153\,\mathrm{d}^{-1}$. The real ones are $f_\psi = 0.5302\,\mathrm{d}^{-1}$ ($P_\psi = 1.8898\,\mathrm{d}$) and $f_\phi = 0.1905\,\mathrm{d}^{-1}$ ($P_\phi = 5.2493\,\mathrm{d}$). The light curve is shorter than the longer period, and as we can see, it causes difficulty in detecting low-frequency (long-period) signals. The fit of this light curve is relatively precise, despite the wrong guess of the frequencies.

6.4 ID1919

In the periodogram of the light curve, there are three dominant peaks around $1.33\,\mathrm{d}^{-1}$, $1.99\,\mathrm{d}^{-1}$, and $2.75\,\mathrm{d}^{-1}$. The third frequency peak, with a small error, can be twice the first frequency peak. It means that the first two frequencies should be one of the main frequencies. The final guess, given by the good fit, is that the first peak is the rotation and the second is the precession in the S-convention. The precession frequency in the L-convention is the difference between them.

I perform a genetic algorithm run multiple times for this light curve and make statistics over the results. The arithmetic mean frequencies are $f_1 = (1.365 \pm 0.004)\,\mathrm{d}^{-1}$ and $f_2 = (0.623 \pm 0.006)\,\mathrm{d}^{-1}$. The real frequencies are $f_\psi = 1.3585\,\mathrm{d}^{-1}$ and $f_\phi = 0.6284\,\mathrm{d}^{-1}$. The differences are 0.5% and 0.9%. After averaging statistics from several runs, we observe that the results are more precise than the individual results in Table C.4.

6.5 The real data

Finally, for the resulting test, I apply all developed and tested methods on the real data of the asteroid 2012 TC4. From the periodogram of the tumbler light curve, I found the set of three dominant frequencies, and by the fit, I searched for the right combination of the precession and rotation frequency. The modeling results are in the Appendix D.

I chose the short-period tumbler 2012 TC4 from the database DAMIT for this test. I take one light curve of the asteroid to calculate the periodogram and fit the data. The final fit of this light curve has frequencies (periods) $f_1 = 2.1469\,\mathrm{h}^{-1}$ ($P_1 = 0.4658\,\mathrm{h}$) and $f_2 = 7.0578\,\mathrm{h}^{-1}$ ($P_2 = 0.1417\,\mathrm{h}$). The real frequencies (periods) are $f_\psi = 2.1810\,\mathrm{h}^{-1}$ ($P_\psi = 0.4585\,\mathrm{h}$) and $f_\phi = 7.0621\,\mathrm{h}^{-1}$ ($P_\phi = 0.1416\,\mathrm{h}$). The differences in periods are 1.6% and 0.07%. The error in the second period (precession) is negligible, but the error in the rotation period is slightly higher. The fit shows that the algorithm did not find the global minimum of the χ^2 function, but it is close. From the periodogram, it was hard to say and find the frequencies. One of the problems can be noise, and also a non-calibrated dataset. The problem with genetic algorithm fitting was the absence of errors in the individual data points. I use the same error for all points. It is also the way to improve the fit and search periods, because of the weighting of the points.

In comparison to the periodogram of the synthetic light curve, this periodogram is more complex with more peaks, harmonic frequencies, and linear combinations. The synthetic light curves were generated by the triaxial ellipsoid, but the real asteroid has a more complex shape. It caused more harmonic frequencies and noise to be present in the periodogram.

6.6 General discussion

Across all tested cases, the genetic algorithm consistently approximated rotational and precessional periods with varying degrees of success. The algorithm converges closely to real values for longer and cleaner light curves. In the shorter and noisier light curves, accuracy is worse, especially for finding long periods (low frequency). This implies that the length of the light curve strongly affects the ability to detect the frequencies correctly. Frequencies usually detected by periodogram must be in the interval from $f_{\min} = 1/T$ to Nyquist's limit frequency. It means that the length of the light curve limits the lower frequency, and the sampling frequency gives the upper limit.

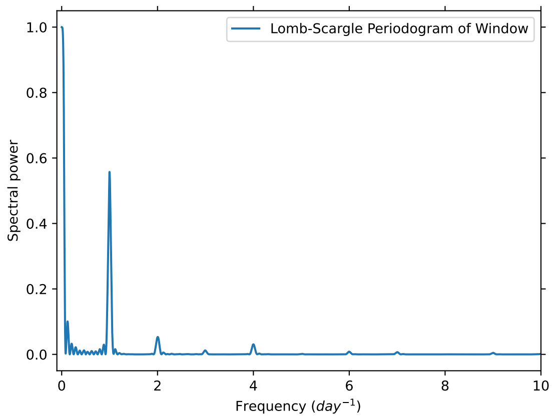

Figure 6.1: Spectral window of the light curve ID1915. The most dominant peak is around $f = 1.00\,\mathrm{d}^{-1}$.

In all light curves, aliasing is present, but it is most evident in ID1915, which directly demonstrates the nighttime observation. In the Figure 6.1, the Spectral window of the light curve ID 1915, calculated by the Lomb-Scargle periodogram, is shown. The strongest peak in the spectral window is around $f_{\mathrm{W}} \approx 1.00\,\mathrm{d}^{-1}$, which directly corresponds with the Earth's rotation period. In the periodogram of the light curve ID1915, we detect strong aliasing. For all three dominant peaks, there also exist significant peaks shifted by approximately $f_{\mathrm{W}}, 2f_{\mathrm{W}}, 3f_{\mathrm{W}}$. In the other spectral window, the most dominant peaks do not have such high amplitude.

In all light curves, the different peaks are prominent. Knowing the true periods in every light curve, I examine the frequency peaks and detect which linear combinations of accurate frequencies they are. The table of these performing frequencies is in Table 6.1. Frequencies were also checked for minor errors and differences.

We see a similar set of frequency peaks in all the light curves. Typical peaks are mainly the f_ψ, f_{ϕ_L} and f_{ϕ_S} or their double frequencies. By looking at the periodogram, we find that the different peaks have different relative heights among the light curves.

Table 6.1: Linear combinations of true frequencies in the LS periodograms of all light curves.

Light curve	Peaks
ID1913	$f_{\phi_L}, f_\psi, 2f_\psi, f_{\phi_S}$
ID1915	$f_{\phi_L}, f_\psi, 2f_\psi, f_{\phi_S}$
ID1916	$2f_{\phi_L}, f_{\phi_S}, 2f_{\phi_S}$
ID1917	$f_{\phi_L}, f_\psi, 2f_\psi, f_{\phi_L}, 2f_{\phi_L}$
ID1916_long	$f_\psi, f_{\psi_S}, 2f_\psi, 2f_{\phi_S}$
ID1918	$f_\psi, 2f_{\phi_S} - f_{\phi_L}$
ID1919	$f_\psi, 2f_\psi, f_{\phi_S}, 2f_{\phi_S}$

7 Conclusion

In this thesis, I investigate the various methods for searching frequencies (periods) in the light curves of tumbling asteroids. I examine the classical periodogram, the CLEAN algorithm, the general Lomb-Scargle periodogram, and modeling by genetic algorithm. I apply these methods to various synthetic light curves of different asteroids with different sampling frequencies, noise, or lengths.

Tumbling asteroids perform a complex rotation that includes rotation and precession—these physical movements of the asteroid cause the non-periodic light curve.

First, I use the CLEAN Fourier periodogram and the general Lomb-Scargle periodogram to detect the most prominent frequencies in the light curve. The CLEAN algorithm iteratively subtracts the peaks from the dirty spectrum and creates the spectrum from clean peaks. It improves the resolution of the frequency peaks and removes the artifacts caused by the sampling. The Lomb-Scargle periodogram is a general periodogram suitable for unevenly sampled data.

Using the periodograms has various limitations. The first limitation is the range of frequencies we can detect in the light curve. Frequencies are limited by the length of the light curve and by the sampling rate. Another difficulty in searching for frequencies is aliasing.

One of the primary goals of the thesis was to examine the peaks in the tumbler's periodogram. We can typically see the complex set of peaks in the periodogram of a tumbler because of its complex rotation. Typical frequencies in the periodogram are rotation frequency, precession frequency, or their various multiples and linear combinations. Thanks to the mathematical description of the movements in S and L conventions, we know the relations between the frequencies and can identify them in the periodogram. Sometimes identifying them is not straightforward and unambiguous, especially in short light curves, periodograms with strong aliasing, etc.

I use a genetic algorithm to fit the light curve to verify the found frequencies. Because of having the first approximation of the frequencies from the periodogram, we can reduce the size of the parametric space, which leads to faster convergence of the genetic algorithm. For the proper run of the genetic algorithm, it is also important to set accurate values for other parameters, such as the number of individuals in a generation, the probability of mutation and crossover, and, importantly, choose the accurate selection method. As I discovered for this problem, the rank-based selection method is better than the widely used roulette selection because of the high number of local extremes in parametric space.

The quality of the periodogram—and consequently the genetic algorithm fit—depends on factors such as noise, data gaps, and sampling frequency. Additionally, the accuracy of the genetic algorithm fit is influenced by how well the initial frequency estimates are guessed from the periodogram. I figure that a good agreement with data is found, calculating the periodogram of several light curves of the same body (in this thesis, light curves ID1916, ID1917, ID1916_long). Typically, slightly different peaks are calculated from each light curve, which helps find the frequencies, detect aliasing, and noise. In case of longer light curves (ID1913, ID1915), more peaks are shown in the periodogram, and it can also help to detect the lower frequencies, unlike the shorter light curve (ID1918), where the lower frequencies cannot be searched.

I also used all the described methods for the real data of the tumbler 2012 TC4. I chose one light curve with length 2.73 h (349 data points). The light curve spans multiple rotational periods, making it suitable for frequency analysis. By the genetic algorithm fit, I found two periods. Compared to the periods in the paper (Lee et al., 2021), it differs slightly, and it implies that the algorithm did not find the global minimum of the χ^2 function, and it should have been run longer. For a better fit, it is also possible to use the Fourier series with a higher order, but not so high, to prevent overfitting or fitting the noise. This light curve is significant because it is long enough to detect both periods and their linear combinations, and the sampling frequency is high enough to detect higher frequencies.

7.1 Future work

As the presented periodograms and the genetic algorithm show, it isn't easy to unambiguously search for and verify the rotation and precession frequency. This method can search for resulting frequencies, after which, it is necessary to prove it by physical modeling of the asteroid rotation by a triaxial ellipsoid or a more complex shape model. As a future improvement, automating the search for frequencies in the periodogram is possible. The genetic algorithm can be better optimized for faster search for the solution.

Bibliography

Astropy Collaboration. (2022). The Astropy Project: Sustaining and Growing a Community-oriented Open-source Project and the Latest Major Release (v5.0) of the Core Package. *935*(2), Article 167, 167. https://doi.org/10.3847/1538-4357/ac7c74

Blanco, A., Delgado, M., & Pegalajar, M. (2001). A real-coded genetic algorithm for training recurrent neural networks. *Neural Networks*, *14*(1), 93–105. https://doi.org/https://doi.org/10.1016/S0893-6080(00)00081-2

Buranský, S. (2023). Analýza komplexních světelných křivek planetek [online] [SUPERVISOR : Tomáš Henych]. https://is.muni.cz/th/dwrj3/

Du, H., Wang, Z., Zhan, W., & Guo, J. (2018). Elitism and distance strategy for selection of evolutionary algorithms. *IEEE Access*, *6*, 1–1. https://doi.org/10.1109/ACCESS.2018.2861760

Durech, J., Sidorin, V., & Kaasalainen, M. (2010). DAMIT: a database of asteroid models. *513*, Article A46, A46. https://doi.org/10.1051/0004-6361/200912693

Harris, A. W. (1994). Tumbling Asteroids. *icarus*, *107*(1), 209–211. https://doi.org/10.1006/icar.1994.1017

Harris, C. R., Millman, K. J., van der Walt, S. J., et al. (2020). Array programming with NumPy. *Nature*, *585*(7825), 357–362. https://doi.org/10.1038/s41586-020-2649-2

Hunter, J. D. (2007). Matplotlib: A 2D graphics environment. *Computing in Science & Engineering*, *9*(3), 90–95. https://doi.org/10.1109/MCSE.2007.55

Chakrabarty, A. (2015). The hadamard product and the free convolutions. https://arxiv.org/abs/1511.03770

Jebari, K., Madiafi, M., et al. (2013). Selection methods for genetic algorithms. *International Journal of Emerging Sciences*, *3*(4), 333–344.

Kaasalainen, M. (2001). Interpretation of lightcurves of precessing asteroids. *aap*, *376*, 302–309. https://doi.org/10.1051/0004-6361:20010935

Lee, H.-J., Ďurech, J., Vokrouhlický, D., Pravec, P., Moon, H.-K., Ryan, W., Kim, M.-J., Kim, C.-H., Choi, Y.-J., Bacci, P., Pollock, J., &

Apitzsch, R. (2021). Spin Change of Asteroid 2012 TC4 Probably by Radiation Torques. *161*(3), Article 112, 112. https://doi.org/10.3847/1538-3881/abd4da

Lomb, N. R. (1976). Least-Squares Frequency Analysis of Unequally Spaced Data. *39*(2), 447–462. https://doi.org/10.1007/BF00648343

McKinney, W. (2010). Data Structures for Statistical Computing in Python. In S. van der Walt & J. Millman (Eds.), *Proceedings of the 9th Python in Science Conference* (pp. 56–61). https://doi.org/10.25080/Majora-92bf1922-00a

Moore, D., McCabe, G., & Craig, B. (2016). *Introduction to the practice of statistics*. W. H. Freeman. https://books.google.cz/books?id=pp-jDgAAQBAJ

Pravec, P., Harris, A., Scheirich, P., Kušnirák, P., Šarounová, L., Hergenrother, C., Mottola, S., Hicks, M., Masi, G., Krugly, Y., Shevchenko, V., Nolan, M., Howell, E., Kaasalainen, M., Galád, A., Brown, P., DeGraff, D., Lambert, J., Cooney, W., & Foglia, S. (2005). Tumbling asteroids [Hapke Symposium]. *Icarus*, *173*(1), 108–131. https://doi.org/https://doi.org/10.1016/j.icarus.2004.07.021

Press, W. H. (2007). *Numerical recipes : The art of scientific computing* (3rd ed.). Cambridge University Press.

Roberts, D. H., Lehar, J., & Dreher, J. W. (1987). Time series analysis with CLEAN. I. Derivation of a spectrum. *aj*, *93*, 968–989. https://doi.org/10.1086/114383

Samarasinha, N. H., & Mueller, B. E. A. (2015). Component periods of non-principal-axis rotation and their manifestations in the lightcurves of asteroids and bare cometary nuclei. *icarus*, *248*, 347–356. https://doi.org/10.1016/j.icarus.2014.10.036

Scargle, J. D. (1982). Studies in astronomical time series analysis. II. Statistical aspects of spectral analysis of unevenly spaced data. *263*, 835–853. https://doi.org/10.1086/160554

VanderPlas, J. T. (2018). Understanding the Lomb-Scargle Periodogram. *236*(1), Article 16, 16. https://doi.org/10.3847/1538-4365/aab766

Vokrouhlický, D., Bottke, W. F., Chesley, S. R., Scheeres, D. J., & Statler, T. S. (2015). The yarkovsky and yorp effects. In *Asteroids iv*. University of Arizona Press. https://doi.org/10.2458/azu_uapress_9780816532131-ch027

A Code

The `Tumbler lightcurve analysis` project is a Python-based toolkit designed to study non-principal-axis (NPA) rotating bodies, commonly referred to as tumblers. The central part of the project involves analyzing tools as described in Chapter 4. In the implementation of the project, several Python packages were used, such as `NumPy`(C. R. Harris et al., 2020), `Pandas` (McKinney, 2010), `AstroPy` mainly for the Lomb-Scargle periodogram (Astropy Collaboration, 2022), and `Matplotlib` for visualizations (Hunter, 2007).

A.1 Project and Structure

The main parts of the project are:

```
Tumbler_lightcurves_analysis
│   ├── main.py
│   └── service.py
├── genetic_algorithm
│   ├── core
│   │   ├── crossover
│   │   ├── fitness_evaluation
│   │   ├── initial_population
│   │   ├── mutation
│   │   └── selection
│   ├── generation
│   └── run
├── periodogram
│   ├── clean_periodogram
│   └── lomb_scargle
└── utils
    ├── find_maxima
    ├── fourier_series_value
    ├── load_dataset
    └── single_fourier_series_value
```

The implementation of the project `Tumbler lightcurve analysis` itself is available on GitHub https://github.com/SBuransky/Tumbler_lightcurves_analysis/releases/tag/v1.0.0 or in the Information system of Masaryk University https://is.muni.cz/auth/th/xlrmb/Tumbler_lightcurves_analysis-1.0.0.zip.

A.2 Usage

The project is developed in `Python 3.10` and requires several additional libraries. To install all necessary dependencies, it is recommended to use the provided `requirements.txt` file. Installation can be performed using `pip`:

```
pip install -r requirements.txt
```

To run the analysis, use the script `main.py` and customize it. Firstly, load your data using this part. Set the name of your file, an appendix of your file, and the names of the columns (but preferably do not change them).

```
name = "ID1913"

data = load_data(
    name,
    column_names=("julian_day", "noisy_flux", "
        deviation_used"),
    appendix=".txt",
)
```

If you want to run periodogram analysis, in this part of the script, change parameters n_iter, n_B for a number of points in the periodogram and final_noise for managing the CLEAN algorithm:

```
tumbler_periodogram(
    data["julian_day"].values,
    data["noisy_flux"].values,
    name=name,
    n_iter=500,
    n_b=10,
    gain=0.5,
    final_noise=0.000008,
    dev=data["deviation_used"],
    x_border=(-0.1, 10),
)
```

and in a terminal run
`python main.py --periodogram`

If you want to run genetic algorithm analysis, change this part of the script:

```
m_ = 2

def fitness(solution):
    x, y, delta = (
        data["julian_day"],
        data["noisy_flux"],
        data["deviation_used"],
    )
    y_model = double_fourier_sequence(solution,
       m_, x)
    chi2 = np.sum((y - y_model) ** 2 / delta**2)
    return 1 / chi2

tumbler_genetic_algorithm_fit(
    data,
    fitness,
    m_=m_,
    population_size=200,
    num_genes=2 * m_ + 2 * m_ * (2 * m_ + 1) +
       4,
    gene_range=(
        [(-0.04, 0.04)] * (m_ * (2 * m_ + 1))
        + [(-0.04, 0.04)] * (m_ * (2 * m_ + 1))
        + [(-0.04, 0.04)] * m_
        + [(-0.04, 0.04)] * m_
        + [
            (0.98, 1.02),
            (-0.00001, 0.00001),
            (0.95, 1.05),   #phi
            (0.65, 0.75),]  #psi
            ),
    name=name,
    num_generations=10000,
    elitism=2,
    mutation_rate=0.01,
```

```
    mutation_range=np.concatenate(
        (
            np.full(m_ * (2 * m_ + 1), 0.05),
            np.full(m_ * (2 * m_ + 1), 0.05),
            np.full(m_, 0.05),
            np.full(m_, 0.05),
            np.array([0.02, 0.000001, 0.04,
               0.04]),
        )
            ),
    limit_fitness=0.001,
)
```

For managing the genetic algorithm run, adjust the population_size, order of the Fourier series m_, gene_range, depending on the estimations of the frequencies, num_generations, elitism, mutation_rate, crossover_rate and mutation_range.

B Results

B.1 ID1917, $s = 0.01$

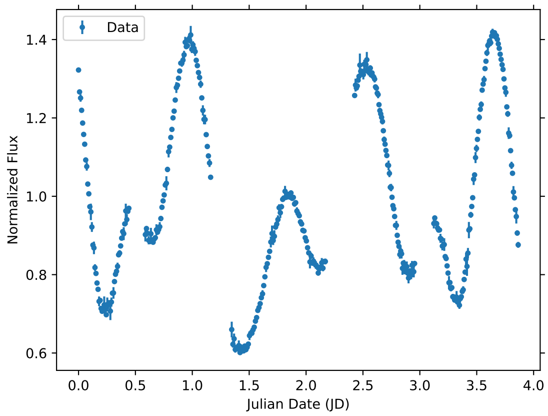

Figure B.1: Synthetic tumbler light curve ID1917 with standard deviation $s = 0.01$

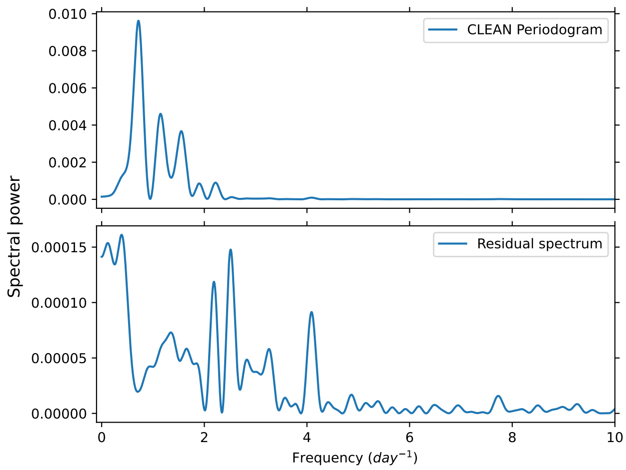

Figure B.2: Clean Fourier periodogram of light curve ID1917 with $s = 0.01$. The most dominant peaks are on frequencies $0.7168\,\mathrm{d}^{-1}$ and $1.1476\,\mathrm{d}^{-1}$.

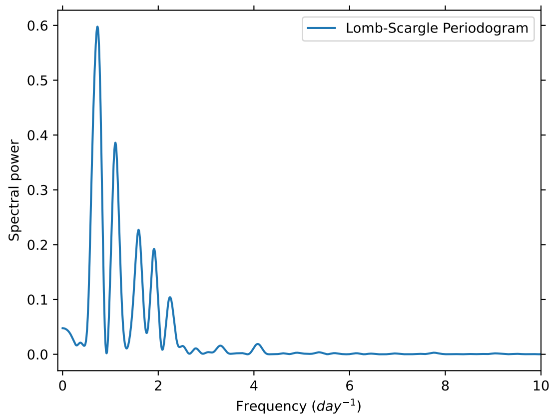

Figure B.3: Lomb-Scargle periodogram of light curve ID1916 with $s = 0.01$. The most dominant peaks are on frequencies $0.7297\,\mathrm{d}^{-1}$ and $1.1036\,\mathrm{d}^{-1}$. The dominant peak in the Spectral window is on frequency $0.3661\,\mathrm{d}^{-1}$.

B.2 ID1916_long, $s = 0.01$

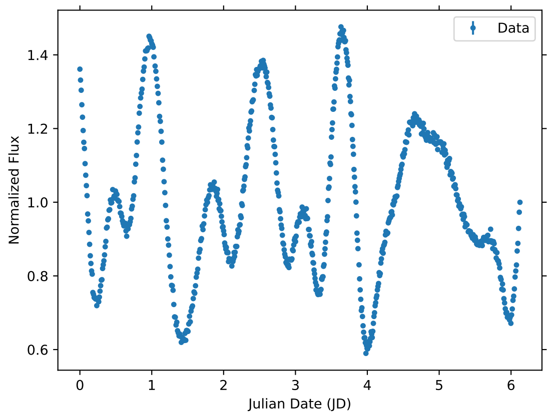

Figure B.4: Synthetic tumbler light curve ID1917 with standard deviation $s = 0.01$

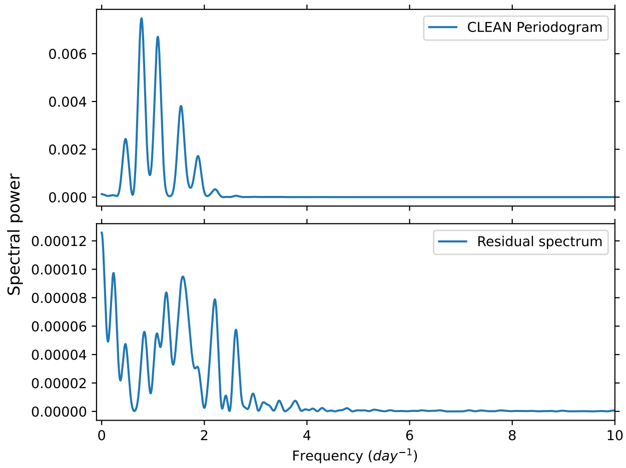

Figure B.5: Clean Fourier periodogram of light curve ID1916_long with $s = 0.01$. The most dominant peaks are on frequencies $0.7756\,\mathrm{d}^{-1}$ and $1.0940\,\mathrm{d}^{-1}$.

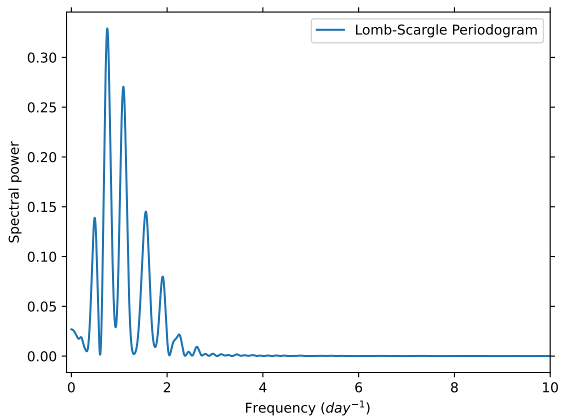

Figure B.6: Lomb-Scargle periodogram of light curve ID1916 with $s = 0.01$. The most dominant peaks are on frequencies $0.7511\,\mathrm{d}^{-1}$ and $1.0858\,\mathrm{d}^{-1}$. The dominant peak in the Spectral window is on frequency $0.2408\,\mathrm{d}^{-1}$.

C More results

C.1 ID1913

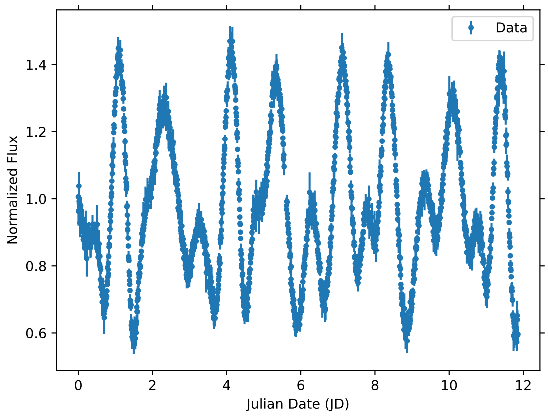

Figure C.1: Synthetic tumbler light curve ID1913.

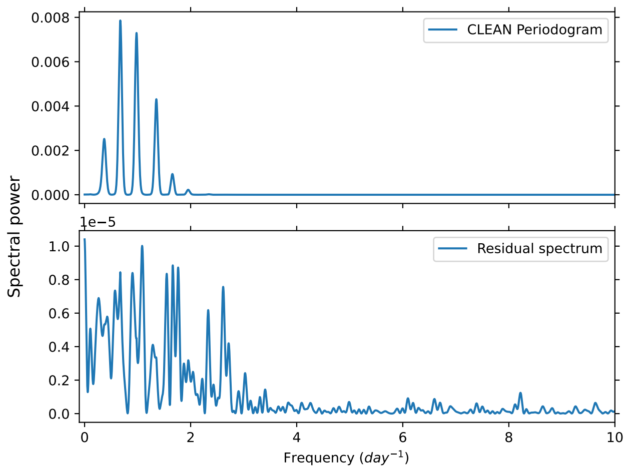

Figure C.2: Clean Fourier periodogram of light curve ID1913. The most dominant peaks are on frequencies 0.3703 d^{-1}, 0.6731 d^{-1}, 0.9793 d^{-1} and 1.3530 d^{-1}.

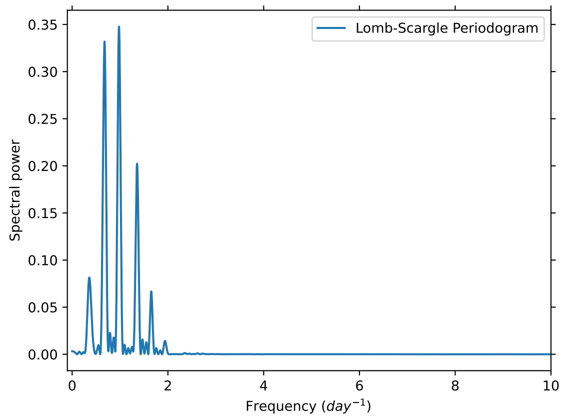

Figure C.3: Lomb-Scargle periodogram of light curve ID1913. The most dominant peaks are on frequencies $0.3585\,\mathrm{d}^{-1}$, $0.6765\,\mathrm{d}^{-1}$, $0.9784\,\mathrm{d}^{-1}$ and $1.3554\,\mathrm{d}^{-1}$. The dominant peak in the Spectral window is on frequency $0.1231\,\mathrm{d}^{-1}$.

The first noticeable thing is that the sum of the first two peaks gives us the third peak. This implies that the first peak can correspond to the precession frequency in L-convention, the second rotational frequency, and the third precession in S-convention. So, as the first guess of the frequencies, I use $f_1 \approx 0.65\,\mathrm{d}^{-1}$ and $f_2 \approx 0.30\,\mathrm{d}^{-1}$.

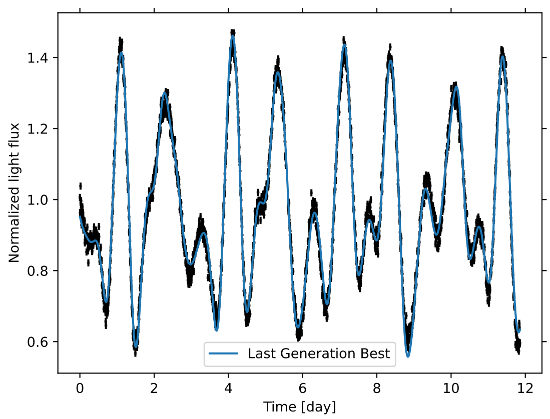

Figure C.4: Fit by genetic algorithm of light curve ID1913

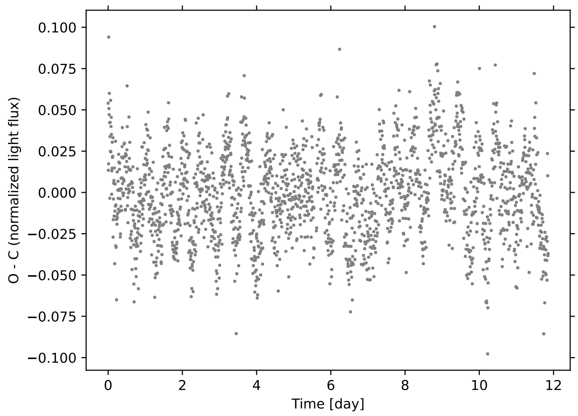

Figure C.5: $O - C$ graph of genetic algorithm fit of light curve ID1913

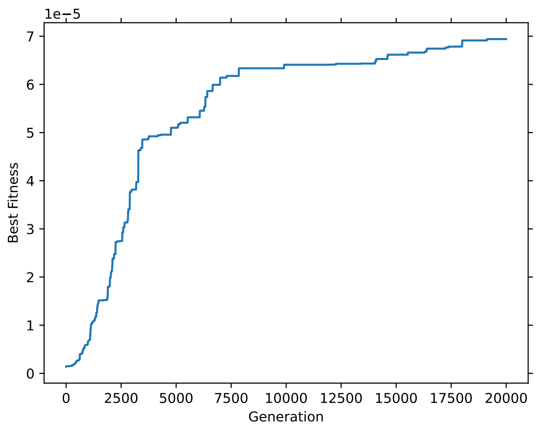

Figure C.6: Fitness evolution of genetic algorithm fit of light curve ID1913

Table C.1: Parameters of genetic algorithm fit of light curve ID1913.

Number of individuals	300	
Number of generations	20 000	
Order of Fourier series	3	
Number of data points	2 000	
χ^2	14 400	
	Calculated	Real
Frequency f_1 [day^{-1}]	0.6803	0.6974
Frequency f_2 [day^{-1}]	0.3211	0.2979
Period P_1 [hours]	35.2786	34.4135
Period P_2 [hours]	74.7431	80.5639

C.2 ID1915

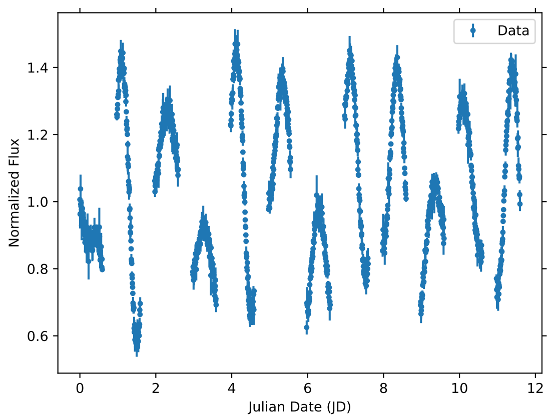

Figure C.7: Synthetic tumbler light curve ID1915.

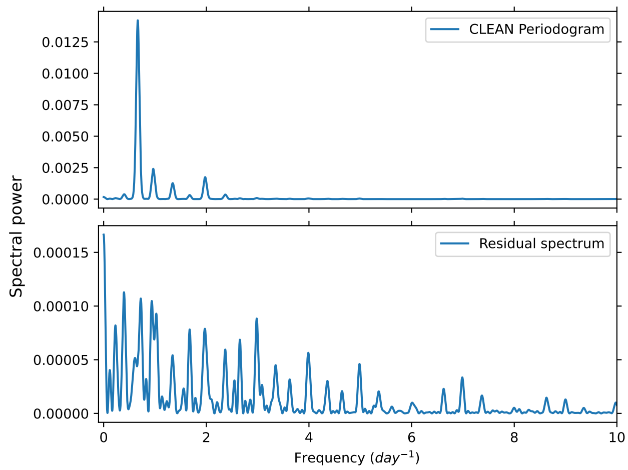

Figure C.8: Clean Fourier periodogram of light curve ID1915. The most dominant peaks are on frequencies $0.6642\,\mathrm{d}^{-1}$ and $0.9661\,\mathrm{d}^{-1}$.

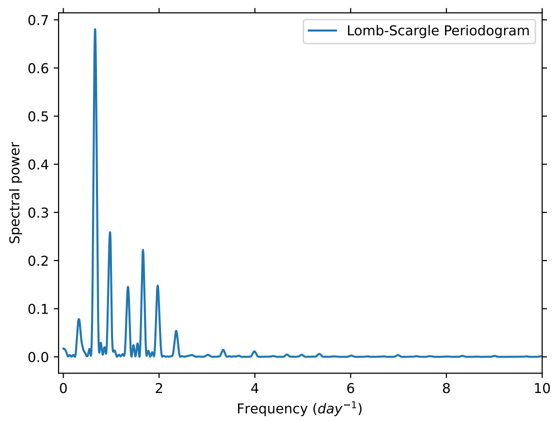

Figure C.9: Lomb-Scargle periodogram of light curve ID1915. The most dominant peaks are on frequencies $0.3243\,\mathrm{d}^{-1}$, $0.6633\,\mathrm{d}^{-1}$, $0.9756\,\mathrm{d}^{-1}$, $1.3499\,\mathrm{d}^{-1}$, $1.6631\,\mathrm{d}^{-1}$ and $1.9701\,\mathrm{d}^{-1}$. The dominant peak in the Spectral window is on frequency $0.9980\,\mathrm{d}^{-1}$.

C.3 ID1918, $s = 0.07$

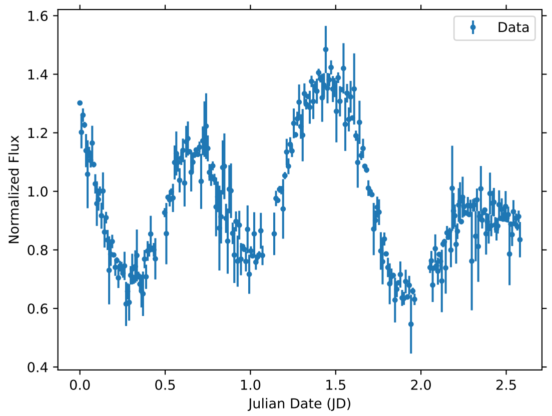

Figure C.10: Synthetic tumbler light curve ID1918 with standard deviation $s = 0.07$

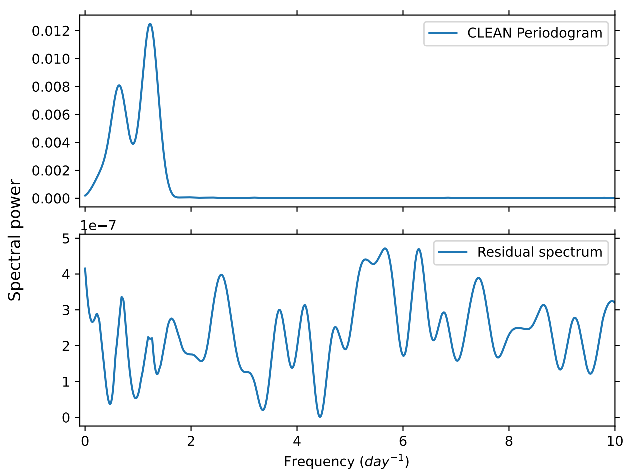

Figure C.11: Clean Fourier periodogram of light curve ID1918 with $s = 0.07$. The most dominant peaks are on frequencies $0.6433\,\mathrm{d}^{-1}$ and $1.2265\,\mathrm{d}^{-1}$.

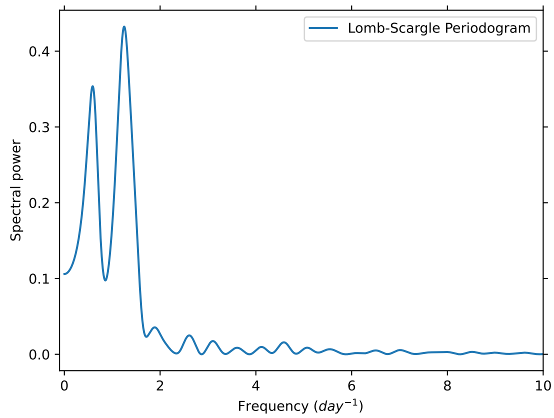

Figure C.12: Lomb-Scargle periodogram of light curve ID1918 with $s = 0.07$. The most dominant peaks are on frequencies $0.5910\,\mathrm{d}^{-1}$ and $1.2497\,\mathrm{d}^{-1}$. The dominant peak in the Spectral window is on frequency $0.5503\,\mathrm{d}^{-1}$.

The two prominent peaks in the periodogram are around $0.60\,\mathrm{d}^{-1}$ and $1.25\,\mathrm{d}^{-1}$. I try more combinations of guessed frequencies; one of the fits follows the half frequencies of the dominant peaks in the periodogram.

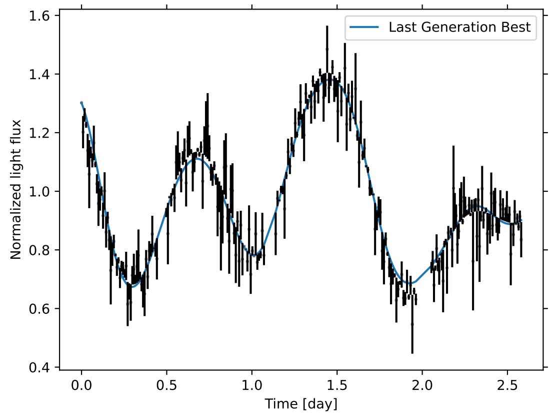

Figure C.13: Fit by genetic algorithm of light curve ID1918 with $s = 0.07$

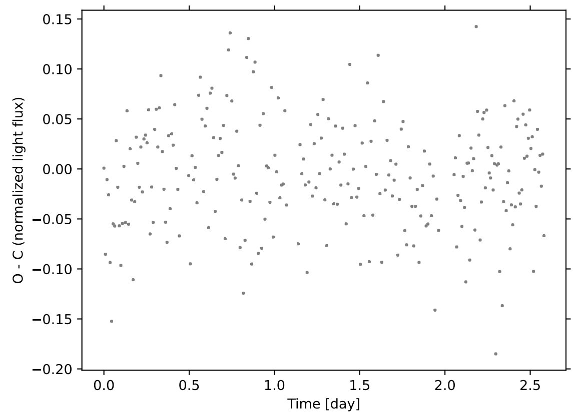

Figure C.14: $O - C$ graph of genetic algorithm fit of light curve ID1918 with $s = 0.07$

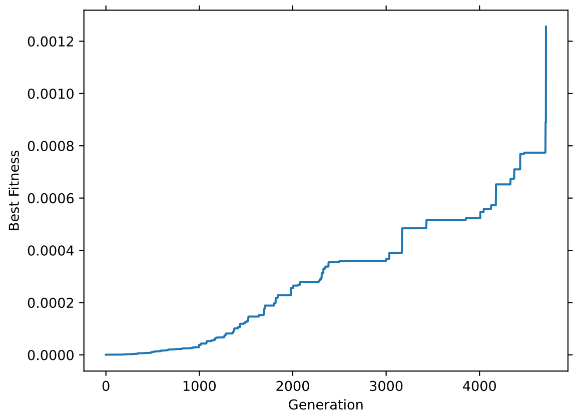

Figure C.15: Fitness evolution of genetic algorithm fit of light curve ID1918 with $s = 0.07$

Table C.2: Parameters of genetic algorithm fit of light curve ID1918 with $s = 0.07$.

Number of individuals	250	
Number of generations	4 712	
Order of Fourier series	3	
Number of data points	260	
χ^2	796	
	Calculated	Real
Frequency $f_1[\text{day}^{-1}]$	0.3313	0.5302
Frequency $f_2[\text{day}^{-1}]$	0.6153	0.1905
Period $P_1[\text{hours}]$	72.4419	45.2659
Period $P_2[\text{hours}]$	39.0054	125.9843

C.4 ID1919, $s = 0.03$

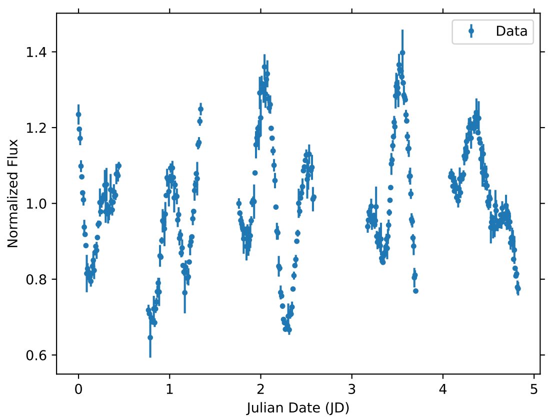

Figure C.16: Synthetic tumbler light curve ID1919 with standard deviation $s = 0.03$

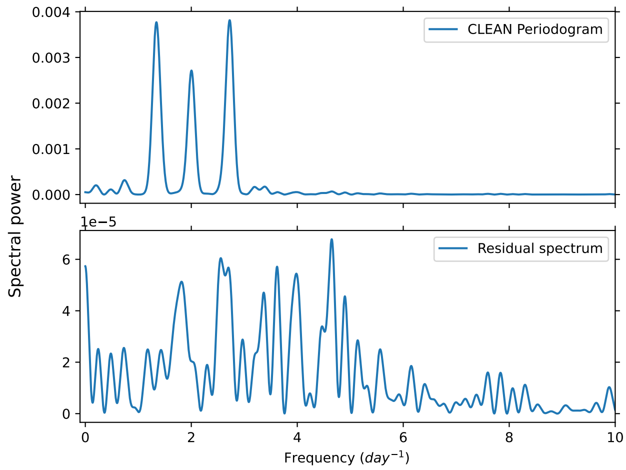

Figure C.17: Clean Fourier periodogram of light curve ID1919 with $s = 0.03$. The most dominant peaks are on frequencies 1.3418 d^{-1}, 2.0028 d^{-1}, 2.7240 d^{-1}.

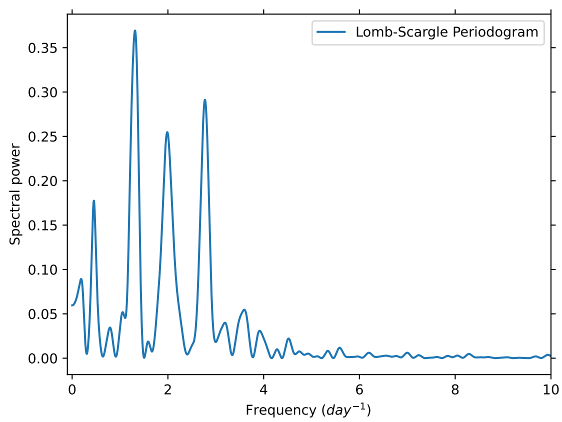

Figure C.18: Lomb-Scargle periodogram of light curve ID1919 with $s = 0.03$. The most dominant peaks are on frequencies 1.3128 d^{-1}, 1.9862 d^{-1}, 2.7737 d^{-1}. The dominant peak in the Spectral window is on frequency 0.8962 d^{-1}.

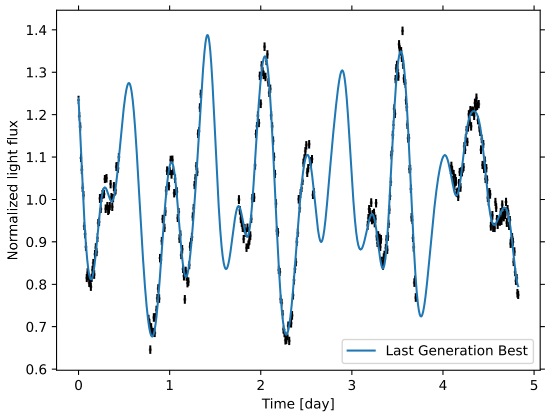

Figure C.19: Fit by genetic algorithm of light curve ID1919 with $s = 0.03$

In this periodogram, I have various estimations of the frequency combination. I obtain the best fit by estimating that the first main peak corresponds to rotation and the second to precession in the S-convention. It means that precession in the L-convention is their difference. I get the guess of the frequencies $f_1 \approx 1.33\,\mathrm{d}^{-1}$ and $f_2 \approx 0.65\,\mathrm{d}^{-1}$.

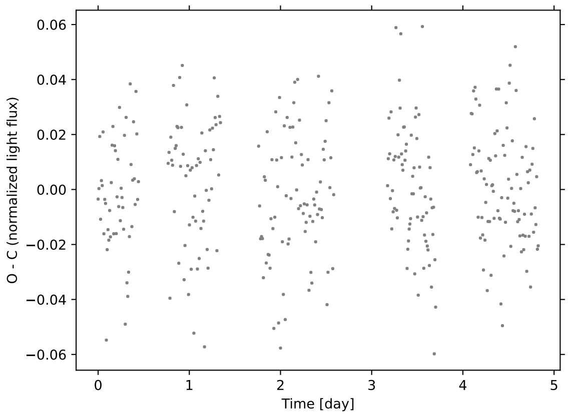

Figure C.20: $O - C$ graph of genetic algorithm fit of light curve ID1919 with $s = 0.03$

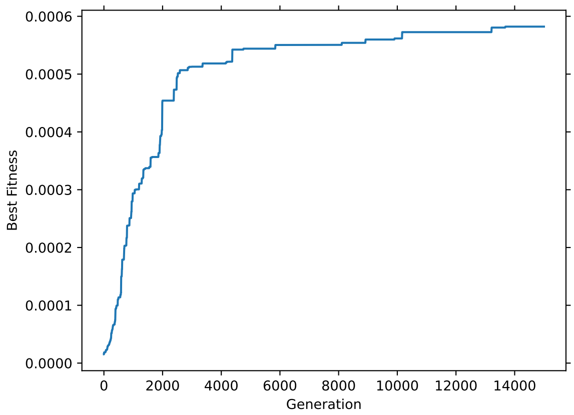

Figure C.21: Fitness evolution of genetic algorithm fit of light curve ID1919 with $s = 0.03$

Table C.3: Parameters of genetic algorithm fit of light curve ID1919 with $s = 0.03$.

Number of individuals	200	
Number of generations	15 000	
Order of Fourier series	3	
Number of data points	350	
χ^2	1 720	
	Calculated	Real
Frequency $f_1\,[\text{day}^{-1}]$	1.3485	1.3585
Frequency $f_2\,[\text{day}^{-1}]$	0.6525	0.6284
Period $P_1\,[\text{hours}]$	17.7976	17.6665
Period $P_2\,[\text{hours}]$	36.7816	38.1922

As described in Section 4.2, I perform a genetic algorithm with the same conditions multiple times, using the same initial conditions, on this problem to obtain statistics over the results and achieve more precise frequencies. These results are in the Table C.4. The arithmetic mean frequencies are $f_1 = (1.36458 \pm 0.004)\,\text{d}^{-1}$ and $f_2 = (0.623 \pm 0.006)\,\text{d}^{-1}$.

Table C.4: Frequencies obtained from multiple runs of the genetic algorithm fit of light curve ID1919 with $s = 0.03$.

$f_1[\mathrm{d}^{-1}]$	$f_2[\mathrm{d}^{-1}]$
1.3491	0.6117
1.3668	0.6420
1.3653	0.5906
1.3485	0.6525
1.3749	0.6259
1.3557	0.6310
1.3757	0.6269
1.3792	0.6083
1.3749	0.6191
1.3557	0.6253

C.5 Bad estimation of frequencies

In this section, I will show how the fits look when the estimated frequencies from the periodogram are some multiples of the real frequencies. In Figure C.22 is the fit of the light curve ID1916 ($s = 0.01$) with final frequencies $f_1 = 0.5853\,\mathrm{d}^{-1}$ and $f_2 = 0.3250\,\mathrm{d}^{-1}$. In reality f_2 is the same but f_1 is higher. These frequencies are approximately half of the peaks in the periodogram. The fit is almost perfect, but the end of the model is increasing, while it should be decreasing and follow the data. It can imply that frequencies are lower than the real ones. The fit is completely inaccurate if the estimation of frequencies is incorrect (not the multiples or sums of real frequencies).

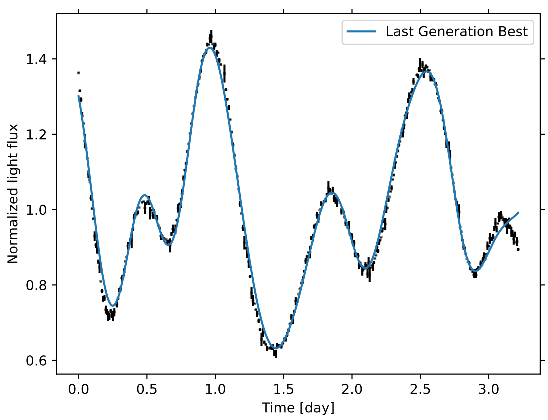

Figure C.22: Fit by genetic algorithm of light curve ID1916 with $s = 0.01$ with bad estimation of the frequencies.

D Testing methods on real data

For the final tests of the presented methods, I use the real data of the asteroid 20112 TC4 from the database DAMIT (Durech et al., 2010).

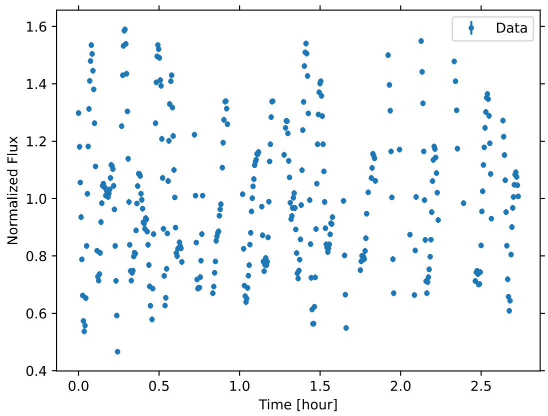

Figure D.1: Light curve of tumbler 2012 TC4.

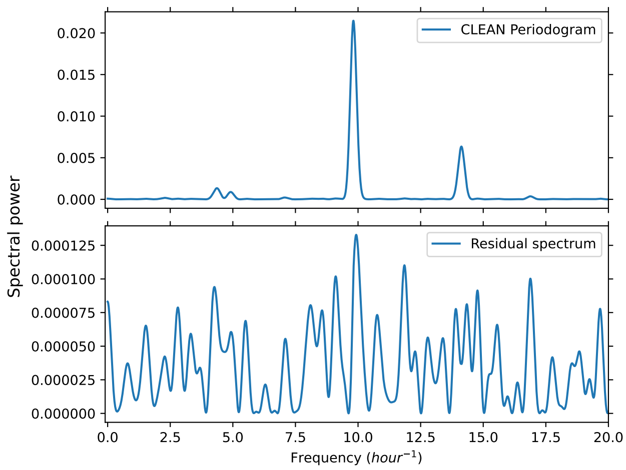

Figure D.2: Clean Fourier periodogram of light curve of tumbler 2012 TC4. The most dominant peaks are on frequencies 4.3663 h^{-1}, 9.8168 h^{-1}, 14.124 54 h^{-1}.

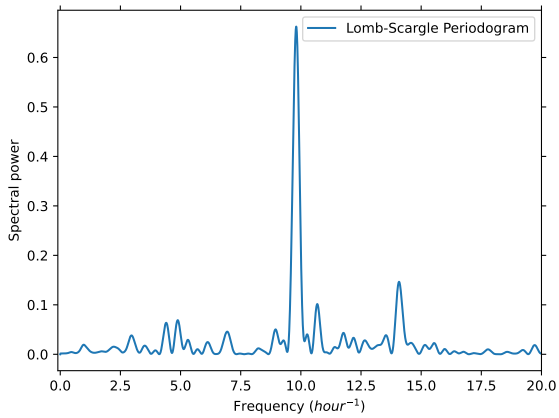

Figure D.3: Lomb-Scargle periodogram of light curve of tumbler 2012 TC4. The most dominant peaks are on frequencies 4.8791 h^{-1}, 6.9377 h^{-1}, 9.8095 h^{-1} and 14.0806 h^{-1}. The dominant peak in the Spectral window is on frequency 0.8938 h^{-1}.

In the tumbler 2012 TC4 periodogram, the most prominent peak corresponds to a frequency of 9.8 h^{-1}. Another significant peak appears around 14.1 h^{-1}. Additionally, the periodogram shows a peak at approximately half of this value, 6.9 h^{-1}, likely indicating a harmonic. The difference between the two lower significant frequencies, 9.8 h^{-1} and 6.9 h^{-1}, is about 2.9 h^{-1}, and both this frequency and its first harmonic (5.9 h^{-1}) are also visible in the periodogram. As a result, three key frequencies stand out: 2.9 h^{-1}, 6.9 h^{-1}, and 9.8 h^{-1}.

It can implies that this three frequencies are the f_{ϕ_L}, f_{ψ}, f_{ϕ_S}. There are two possibilities, and I try to fit and test them both. First is that the lower frequency is the rotation, and the second possibility is that the lower frequency is the precession in the L-convention. The resulting fit is in Figure D.4 and the results are in Table D.1.

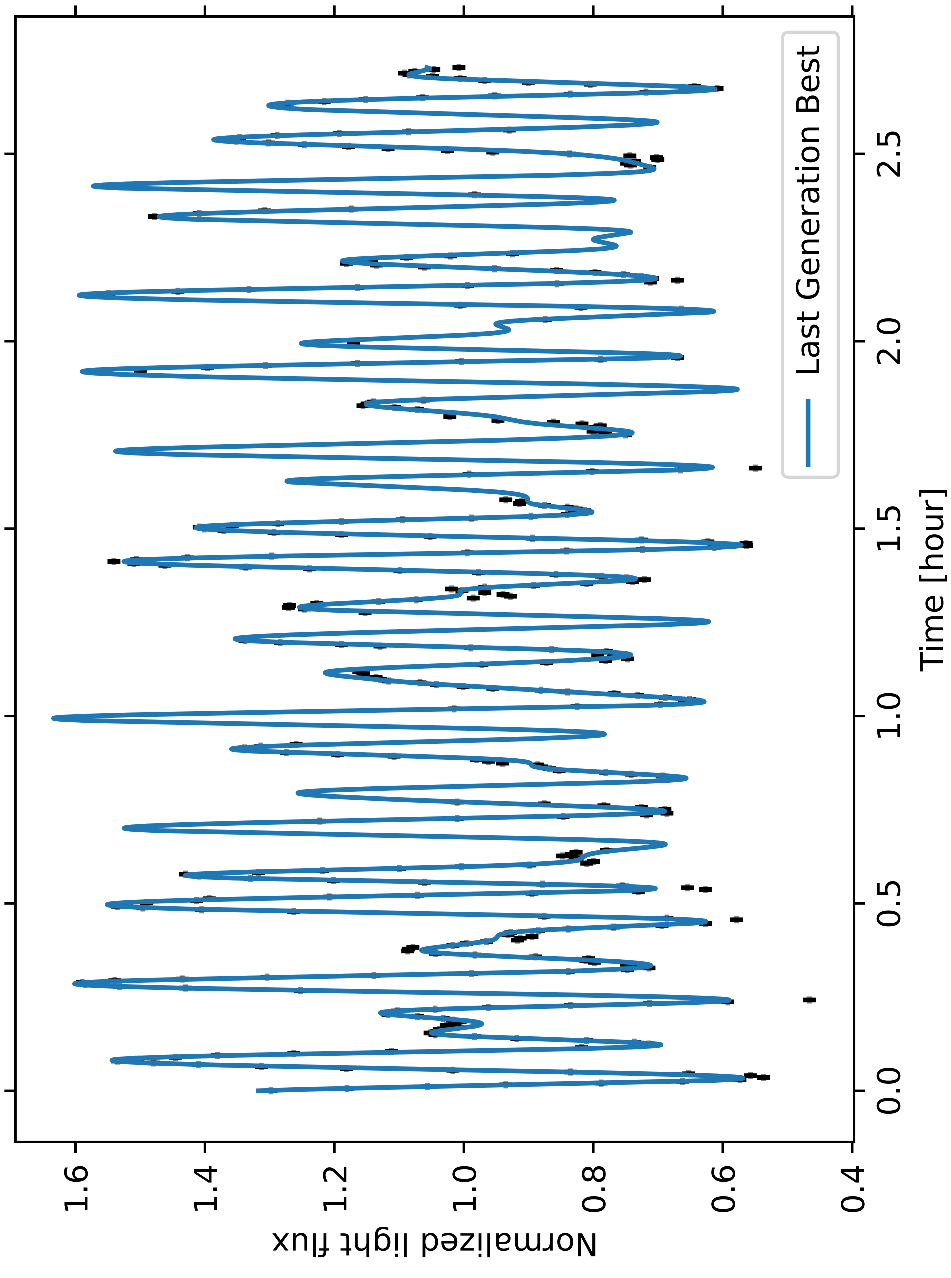

Figure D.4: Fit by genetic algorithm of light curve of tumbler 2012 TC4.

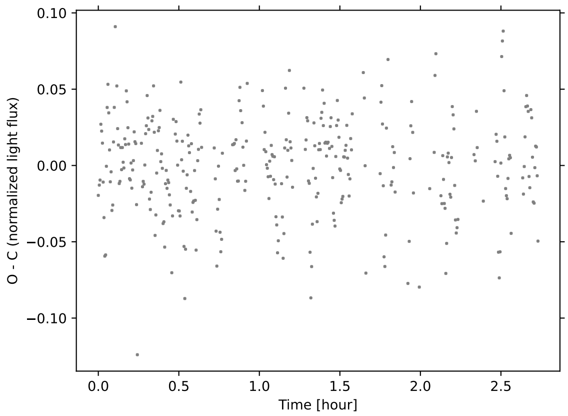

Figure D.5: $O - C$ graph of genetic algorithm fit of light curve of tumbler 2012 TC4.

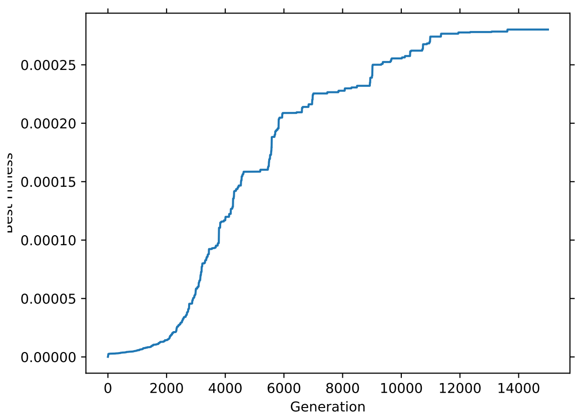

Figure D.6: Fitness evolution of genetic algorithm fit of light curve of tumbler 2012 TC4.

Table D.1: Parameters of genetic algorithm fit of light curve of tumbler 2012 TC4. The real values were taken from (Lee et al., 2021). For the genetic algorithm fitting, I set the same error for all values, 0.01, because of the absence of error in the data.

Number of individuals	250	
Number of generations	15 000	
Order of Fourier series	3	
Number of data points	349	
χ^2	3 570	
	Calculated	Real
Frequency f_1[hour^{-1}]	2.1469	2.1810
Frequency f_2[hour^{-1}]	7.0578	7.0621
Period P_1[hours]	0.4658	0.4585
Period P_2[hours]	0.1417	0.1416